

12

AD A119614

## Studies of Plasma Properties in Rocket Plumes

RICHARD H. C. LEE and I-SHIH CHANG  
Vehicle Engineering Division  
Engineering Group  
and  
GORDON E. STEWART  
Laboratory Operations  
The Aerospace Corporation  
El Segundo, Calif. 90245

17 May 1982

DTIC  
ELECTED  
SEP 27 1982  
H

Interim Report  
(1 April 1981 — 31 March 1982)

APPROVED FOR PUBLIC RELEASE;  
DISTRIBUTION UNLIMITED

Prepared for  
SPACE DIVISION  
AIR FORCE SYSTEMS COMMAND  
Los Angeles Air Force Station  
P.O. Box 92960, Worldway Postal Center  
Los Angeles, Calif. 90009

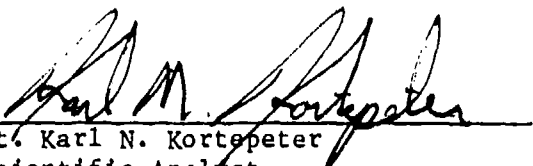
DTIC FILE COPY

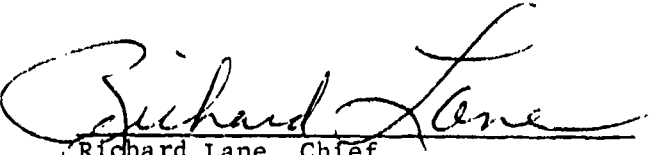
82 09 27 142


This interim report was prepared for the Western Space and Missile Center, Vandenberg AFB, CA 93437 by The Aerospace Corporation, El Segundo, CA 90245, under Contract No. F04701-81-C-0082 with the Space Division, Air Force Systems Command, P.O. Box 92960, Worldway Postal Center, Los Angeles, CA 90009. It was reviewed and approved for The Aerospace Corporation by E. G. Hertler, Principal Director, Aero Engineering Subdivision. First Lieutenant Karl Kortepeter was the Project Engineer for the Analysis Branch, Western Space and Missile Center.

This report has been reviewed by the Public Affairs Office (PAS) and is releasable to the National Technical Information Service (NTIS). At NTIS, it will be available to the general public, including foreign nations.

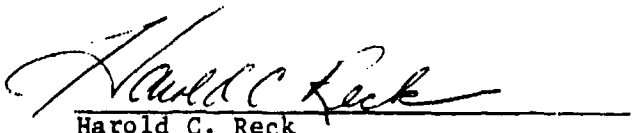
This technical report has been reviewed and is approved for publication. Publication of this report does not constitute Air Force approval of the report's findings or conclusions. It is published only for the exchange and stimulation of ideas.

  
Lt. Karl N. Kortepeter  
Scientific Analyst  
Analysis Branch

  
Richard Lane, Chief  
Analysis Branch

  
Kingston A. George, Chief  
Requirements and Analysis Division

FOR THE COMMANDER

  
Harold C. Reck  
Acting Director of Plans,  
Programs and Requirements

UNCLASSIFIED

SECURITY CLASSIFICATION OF THIS PAGE (When Data Entered)

REPORT DOCUMENTATION PAGE		READ INSTRUCTIONS BEFORE COMPLETING FORM
1. REPORT NUMBER SD-TR-82-44	2. GQVT ACCESSION NO. AD-A119 614	3. RECIPIENT'S CATALOG NUMBER
4. TITLE (and Subtitle) STUDIES OF PLASMA PROPERTIES IN ROCKET PLUMES	5. TYPE OF REPORT & PERIOD COVERED Final Report 1981 to 31 Mar 1982	
7. AUTHOR(s) Richard H.C. Lee, I-Shih Chang, and Gordon E. Stewart	6. PERFORMING ORG. REPORT NUMBER (82) 9-1	
9. PERFORMING ORGANIZATION NAME AND ADDRESS The Aerospace Corporation El Segundo, Calif. 90245	8. C. SPACE OR GRANT NUMBER(s) 704 0082	
11. CONTROLLING OFFICE NAME AND ADDRESS Western Space and Missile Command Vandenberg AFB, CA 93437	12. REPORT DATE 17 May 1982	
14. MONITORING AGENCY NAME & ADDRESS (if different from Controlling Office) Space Division, AFSC Los Angeles Air Force Station P. O. Box 92960 Worldway Postal Center Los Angeles, California 90009	13. NUMBER OF PAGES 60	
	15. SECURITY CLASS. (of this report) Unclassified	
	15a. DECLASSIFICATION DOWNGRADING SCHEDULE	
16. DISTRIBUTION STATEMENT (of this Report) Approved for public release; distribution unlimited		
17. DISTRIBUTION STATEMENT (of the abstract entered in Block 20, if different from Report)		
18. SUPPLEMENTARY NOTES This work was performed in support of the launch operation activities of Western Space and Missile Center at Vandenberg Air Force Base. Lieutenant Karl Kortepeter, WSMC/XRQA, was Project Manager.		
19. KEY WORDS (Continue on reverse side if necessary and identify by block number) Rocket Plume                      Plasma                      Solid Rockets Attenuation                      Radio Frequency Telemetry                      Two-Phase Flow Launch Operations                      MX Missile		
20. ABSTRACT (Continue on reverse side if necessary and identify by block number) Various factors which affect the gas density and electron density distribution in the exhaust plume from solid rocket engines were studied. The particulates affect the plume density distribution through their effects on the nozzle flow field. The two-body attachment reaction $HCl + e = H + Cl^-$ is the dominant reaction in determining the ionization level in the nozzle expansion. The chemical and physical phenomena required to accurately determine the plume plasma properties for subsequent radio frequency interaction analysis are identified.		

DD FORM 1473  
(FACSIMILE)

UNCLASSIFIED

SECURITY CLASSIFICATION OF THIS PAGE (When Data Entered)

# PREFACE

The authors appreciate the efforts provided by George R. Judd of the Information Processing Division, The Aerospace Corporation, in computer programming support.



Accession For	
NTIS GRA&I	<input checked="" type="checkbox"/>
DTIC TAB	<input type="checkbox"/>
Unannounced	<input type="checkbox"/>
Justification	
By	
Distribution/	
Availability Codes	
Avail and/or	
Dist	Special
A	

## CONTENTS

PREFACE . . . . .	1
1. INTRODUCTION . . . . .	9
2. METHODOLOGY OF RF-PLUME PLASMA INTERACTION ANALYSIS. . . . .	13
2.1 Rocket Engine Characterization and Exit Plume Flow Properties . . . . .	13
2.2 Rocket Plume Flow Field . . . . .	15
2.3 RF-Plume Plasma Interaction . . . . .	17
3. RESULTS. . . . .	21
3.1 Effects of Ionic Reaction Rate. . . . .	21
3.2 Two-Phase Flow in Rocket Nozzle . . . . .	25
3.3 Rocket Exhaust Plume Flow Field . . . . .	44
3.3.1 Approximate Far Field Plume Models . . . . .	44
3.3.2 Effect of Particulates on Plume Electron Density. . . . .	47
3.3.3 Effect of External Atmosphere. . . . .	52
3.3.4 Effect of Nozzle Wall Boundary Layer . . . . .	52
3.3.5 Effect of Nozzle Length. . . . .	54
4. CONCLUSIONS. . . . .	57
REFERENCES . . . . .	59
APPENDIX . . . . .	63

## FIGURES

1. Effect of Two-Body Electron Attachment Rate . . . . .	21
2. Neutral Chemical Species Distribution along Rocket Nozzle . . . . .	26
3. Ionic Species Distribution along Rocket Nozzle. . . . .	27
4. Effect of Integration Step Size on Electron Mole Fraction . . . . .	28
5. MX Third Stage Motor Interior Configuration . . . . .	31
6. Computational Grid for Transonic Flow Regime. . . . .	31
7. Cross-Sectional Grid for Supersonic Flow Regime . . . . .	32
8. Mach Number Contour, Two-Phase (Transonic Regime) . . . . .	33
9. Gas Density Contour, Two-Phase (Transonic Regime) . . . . .	33
10. Mach Number Contour, Two-Phase (Supersonic Regime). . . . .	34
11. Gas Density Contour, Two-Phase (Supersonic Regime). . . . .	34
12. Mach Number Contour, One-Phase (Transonic Regime) . . . . .	35
13. Gas Density Contour, One-Phase (Transonic Regime) . . . . .	35
14. Mach Number Contour, One-Phase (Supersonic Regime). . . . .	36
15. Gas Density Contour, One-Phase (Supersonic Regime). . . . .	36
16. Profiles of Mach Number and Temperature at Nozzle Exit Plane with Single Particle Size of $6.7 \mu\text{m}$ . . . . .	37
17. Profiles of Pressure and Density at Nozzle Exit Plane with Single Particle Size of $6.7 \mu\text{m}$ . . . . .	38
18. Radial Profiles of Gas Temperature and Density at Nozzle Exit . . . . .	40
19. Radial Profiles of Mach Number and Gas Pressure at Nozzle Exit . . . . .	42
20. Effect of Mean Particle Diameter on Exit Mach Number. . . . .	43

## FIGURES (Concluded)

21. Mass Flow along MX Third Stage Plume Axis . . . . .	46
22. Contours of Constant Electron Density for Uniform Exit Mach Number. . . . .	48
23. Electron Density Contours for Gas and Two-Phase Plume . . . . .	50
24. Effect of Two-Phase Nozzle Flow on Gas Plume at 310 kft . . . . .	51
25. Atmospheric Effect of UHF Overdense Contour . . . . .	53
26. Effect of Nozzle Boundary Layer . . . . .	55
27. UHF Overdense Contour of MX Third Stage Plume at 310 kft. . . . .	56

## TABLES

1. Ionic Reactions . . . . .	12
2. Effects of Ionic Reaction Rates on Electron Mole Fraction at Nozzle Exit . . . . .	23
3. Gas and Solid Properties for Two-Phase Nozzle Flow Calculation . . . . .	29



## 1. INTRODUCTION

The objective of this study is to develop the necessary techniques and computer codes to theoretically determine the effects of rocket exhaust plumes on radio frequency (RF) signal propagation between the launch missile and a ground or airborne station. Primary emphasis will be placed on the altitude regime for the third stage solid engine of the MX missile. The focus of the studies conducted thus far were to review various aspects of the state of the art in RF interference from rocket plumes, to study and determine the dominant factors in affecting the plume plasma and in influencing the RF plume interaction, and to define the state-of-the-art models required for its solution. The results and findings are presented in this report.

Continuous communication with a missile during launch is essential for the successful and safe completion of the launch operation. Critical operations, such as target tracking, telemetry transmission, and command-destruct, all depend upon adequate propagation of electromagnetic radiation in the radio wave spectrum from or to the launch vehicle. Unfortunately, it often occurs that the rocket exhaust may be in a high level of ionization which gives rise to free electrons in the exhaust plume. These free electrons can, in many cases, interfere with the propagation of an electromagnetic signal when they are present in sufficiently large amounts and when the line of sight between the missile and the ground antennas traverses the missile plume.

The amount of electrons in the plume is intimately related to the alkali metal impurities in the propellant, for the rocket engine temperature is generally not high enough to cause ionization of the other combustion products. However, because the alkali metals (notably potassium and sodium) have low ionization potentials, they become highly ionized with the result that considerable amounts of electrons are generated and deposited in the exhaust plume. In general, solid rocket propellants contain much larger amounts of sodium and potassium contaminants than liquid propellants. This is mainly due to the

chemical process of manufacturing ammonium perchlorate, an essential ingredient in the solid propellant, which carries over some original raw materials containing alkali metal compounds. While this study is primarily aimed at exhaust plumes from solid rocket engines, the analysis applies to those from liquid rocket engines as well. The principal differences between the two types of rocket plumes lie in the presence of large amounts of particulates in the solid rocket plume and the different chemical composition. Therefore, the ability to calculate solid rocket plumes automatically includes liquid rocket plume by deleting the particular phase in the plume flow field.

RF interferences from rocket plumes have been observed in numerous launch operations in the past. References 1 and 2 provide good summaries of the existing data. More detailed description of field data from various launch sites may be found in Refs. 3 through 9. A large amount of S-band telemetry attenuation data are also available from numerous Minuteman III launches from

- 
- <sup>1</sup>Victor, A.C., "Plume Signal Interference, Part 1: Radar Attenuation," Report NWC-TP-5319, Part 1, Naval Weapons Center, China Lake, CA, June 1985.
  - <sup>2</sup>Victor, A.C., "Plume Signal Interference, Part 1: Plume-Induced Noise (U)," Report NWC-TP-5319, Part 2, Naval Weapons Center, China Lake, CA, June 1975 (Confidential).
  - <sup>3</sup>Poehler, H.A., "Results of Special Flame Measurements of Titan III-C Tests 3656/6025 and 6020/6546," Report ETV-TRM-66-30, Pan American World Airways, Guided Missile Range Division, 1966.
  - <sup>4</sup>Poehler, H.A., "Project See-Thru, Flame Attenuation Interference Measurements, Titan III-C Test 8275/2250, Preliminary Report," Report No. ETR-TR-68-6, Pan American World Airways, 1967.
  - <sup>5</sup>Poehler, H.A., "Project See-Thru, Flame Interference Measurements, Titan III-C Launch Test 8275/2250, Final Report," Report No. ETR-TR-68-3, Pan American World Airways, 1968.
  - <sup>6</sup>Poehler, H.A., "Rocket Exhaust Signal Attenuation and Degradation, Final Report, Vols. I, II, III," Report No. ETR-TR-69-4, Pan American World Airways, Aerospace Service Division, 1969.
  - <sup>7</sup>Ely, O.P., "Rocket Exhaust Effects on Radio Frequency Transmission," J. Spacecraft, 3, pp. 310-314, 1966.
  - <sup>8</sup>Vicente, F.A., E.C. Taylor, and R.W. Phelps, "Analysis of Flame Effects on Measuring Electromagnetic Propagation Data," J. Spacecraft, 4, pp. 1069-1075, 1967.
  - <sup>9</sup>Golden K.E., E.L. Taylor, and F.A. Vicente, "Diffraction by Rocket Exhaust," Communication in IEEE Transaction on Antenna and Propagation, AP16, pp. 614-616, 1968.

Western Test Range (WTR). They were recorded at antenna locations over some distances apart and, therefore, should provide indications of the aspect angle variations of plume interference. They are available as Post-Launch Analysis of Telemetry Systems (PLATS) reports issued by Western Space and Missile Center (WSMC).<sup>10,11</sup>

These data have shown both amplitude and phase interference of the RF signal due to the presence of the rocket exhaust plume. In many instances, both amplitude and phase noise were also detected. It appears that the noise may be due to turbulent fluctuations in the plume plasma. Spectral analysis of the amplitude noise has been made and indicated a peak noise at about 1 kHz.<sup>12</sup>

Although it is necessary to account for amplitude and phase perturbations in the RF signal in the mean values as well as noises to completely define rocket plume effects on RF signal propagation, the initial efforts of this study will be confined to determining the effects on the mean signal amplitude and phase. Only the mean plume flow field properties will be calculated, and the RF-plasma interaction analysis will be restricted to employing the mean plasma properties and determining the mean amplitude and phase changes. This is necessary in order to confine the initial efforts to a tractable level. The inclusion of amplitude and phase noise study will necessitate treating turbulent fluctuations in the rocket plume flow field and may entail studies beyond the present state of the art. It appears that at the altitudes of interest associated with the third stage burn of the MX missile, the turbulence in the rocket plume is mainly originated from the combustion

---

<sup>10</sup>"Post Launch Analysis Telemetry Systems Preview--Operation 3162," Report No. PA300-T-79-31P, Systems Performance Analysis Department, Western Test Range Division, Federal Electric Corporation, 26 July 1979.

<sup>11</sup>"Post Launch Analysis of Telemetry Systems--Operation 5544, Final," Report No. AS300-T-81-21F, Systems Performance Analysis Department, Western Test Range Division, Federal Electric Corporation, 1 April 1981.

<sup>12</sup>McKelvey, G.R., "Exhaust Plume Test Results--Report Number 2," Technical Note PA300-N-79-23, Systems Performance Analysis Department, Western Test Range Division, Federal Electric Corporation, 27 September 1979.

chamber of the rocket engine and retained by the core flow of the plume. This is in contrast to plume turbulence at low altitudes, such as during the first stage burn, where the dominant plume turbulence is generated by the free shear layer between the plume gas and the ambient air. While a limited amount of data of turbulent fluctuations in the plume core does exist,<sup>13,14</sup> it pertains to those from a liquid rocket engine of small thrust. Applications to solid rocket engines and higher thrust levels require further study. The inclusion of plume turbulence is beyond the scope of the present initial effort.

The results and conclusions of this report consist of various studies and analyses to define the necessary theoretical models and computer codes that determine the RF signal amplitude and phase interference due to rocket plumes.

---

<sup>13</sup>Sutton, G.A., "Boost Measurements and Analysis Program Final Report, Vol. 7: Plasma Properties Derived From Full Scale Rocket Motor Measurements," Ford Aerospace and Communications Corporation Report No. U-6511, prepared by Concord Sciences Corporation, Concord, MS, 15 March 1979.

<sup>14</sup>August G. and D. Tremain, "Boost Measurements and Analysis Program Final Report, Vol. 9: Rocket Plume Measurements and Data Evaluation," Ford Aerospace and Communications Corporation Report No. U-6511, prepared by Concord Sciences Corporation, Concord, MS, 15 March 1979.

## 2. METHODOLOGY OF RF-PLUME PLASMA INTERACTION ANALYSIS

The analyses necessary for determining the plume effects on RF signal propagation are complex and lengthy. It is useful to separate the analyses into a number of sequential calculations for various chemical and physical phenomena:

- o Rocket Engine Characterization and Exit Plane Flow Properties
- o Rocket Plume Flow Field
- o RF-Plume Plasma Interaction

These calculations are briefly described below.

### 2.1 ROCKET ENGINE CHARACTERIZATION AND EXIT PLUME FLOW PROPERTIES

The first step in the analysis is to determine the properties of the rocket engine exhaust at the nozzle exit. The essential data to carry out this calculation are the chemical composition of the rocket propellant including the amount of alkali metal contaminants, the rocket chamber pressure, and the detailed geometrical configuration of the engine chamber, nozzle throat, and nozzle contour.

The availability of the alkali metal contaminant levels in the propellant is essential to the determination of the electron density in the rocket plume. These contaminants are introduced in the propellant mainly via ammonium perchlorate, an essential ingredient in the common solid propellants. A rule of thumb to estimate their content is to assume 200 parts per million (ppm) of potassium and 125 ppm of sodium by weight to be present in the ammonium perchlorate\* and then to compute their weight fraction in the composite

---

\*Private communication with E.M. Landsbaum, The Aerospace Corporation.

propellant. This is only a very crude estimate, however, and it often produces unreliable results. It is imperative that the propellant be chemically analyzed for alkali impurity content to define the weight fraction accurately.

The characterization of the rocket exhaust flow properties begins with a calculation of the rocket engine chamber flow properties and composition by assuming chemical equilibrium to prevail at the specified chamber pressure at a constant enthalpy. Because the flow velocity is low and the chamber temperature is high, the combustion time is very short in comparison with the time required for the combustion products to flow through the entire chamber. Under this condition, chemical equilibrium is attained.

As the combustion products flow into the entrance region of the nozzle throat, their velocities increase rapidly and deviation from chemical equilibrium starts. Therefore, the calculation must consider finite chemical reaction rates as the engine exhaust flows into the throat and is expanded in the rocket nozzle. Since a large amount of particulates is present in the combustion products of solid propellants, it is often necessary to treat two-phase flow in the throat and nozzle calculations.

While a number of computer codes exist for the calculations described in this section, the Solid Performance Program (SPP) code developed under the auspices of the Air Force Rocket Propulsion Laboratory combined them into one code which has been adapted for the present study.

The gas velocity is subsonic in the chamber and becomes supersonic downstream of the nozzle throat. Much attention has been devoted to the method of computing the transonic flow as the two-phase rocket exhaust passes from the chamber to the nozzle. The approximate transonic analysis of the SPP code avoids treating elliptic partial differential equations for the subsonic flow by solving the inlet region of the nozzle as a one-dimensional flow problem. As the exhaust passes through the throat, an uncoupled particle-gas flow with constant fractional thermal and velocity lag was assumed. Solutions from the

SPP code will be compared with the cylindrical three-dimensional two-phase flow (CY3D2P) code<sup>15</sup> developed at The Aerospace Corporation to check the accuracy of the former code. The CY3D2P code treats the fully coupled, unsteady governing equations for both the gas and the particulate phases so as to retain the hyperbolic form of the governing equations. It provides an exact solution to the two-phase flow problem; however, it does so at the expense of additional computing time and storage.

Typical results from the SPP code for the third stage of the MX missile as well as its comparison with the CY3D2P code will be presented later in this report. It is anticipated that when the SPP code is thus validated, it will be adopted for all subsequent calculations.

## 2.2 ROCKET PLUME FLOW FIELD

The next step in the analysis is to take the rocket engine exhaust flow properties at the nozzle exit plane to continue the calculation outside the nozzle. When only gas phase is considered, a number of simplified approximations may be used for the far field of the rocket plume.<sup>16-18</sup> The approximations assume that the gas has been sufficiently expanded outside the nozzle to approach a source-like flow, and the detailed mechanisms of the gas expansion in the vicinity of the nozzle are of minor importance. Their ability to describe the plume gas density distribution was investigated. Also, in the low altitude regime of the MX third stage burn for the BOA3 trajectory, interaction between the plume gas and the ambient atmosphere becomes important in

---

<sup>15</sup>Chang, I-S., "Three-Dimensional, Two-Phase Supersonic Nozzle Flows," AIAA Paper No. 81-1219, AIAA 14th Fluid and Plasma Dynamics Conference, Palo Alto, CA, 23 June 1981.

<sup>16</sup>Hill, A.F.J. and J.S. Draper, "Analytical Approximation for the Flow from a Nozzle into a Vacuum," J. Spacecraft, 3, pp. 1552-1554, 1966.

<sup>17</sup>Brook J.W., "Far Field Approximation for a Nozzle Exhausting into a Vacuum," J. Spacecraft, 6, pp. 626-628, 1969.

<sup>18</sup>Boynton, F.P., "Exhaust Plumes from Nozzles with Wall Boundary Layers," J. Spacecraft, 5, pp. 1143-1147, 1968.

affecting the plume plasma properties. The interaction generates the bow shock and the barrel shock in the plume. Its effect on the plume shape was considered. The method of characteristics (MOC) solution<sup>19</sup> has been applied to the inviscid flow of plume in the past with some success and was used in this study to compute the plume flow field and plasma properties. It has the capability of treating the barrel shock formation while assuming modified Newtonian pressure at the plume boundary.

When the presence of particulates in the plume needs to be considered, the computation becomes more complex and lengthy. Two computer codes are available for calculating two-phase plume flow fields by the method of characteristics, namely, the Reacting Multi-Phase Code (RAMP)<sup>20,21</sup> and the Two-Dimensional Two-Phase Plume Analysis Program (TD2P).<sup>22,23</sup> The latter code was used in this work to study the effects of particulates on the plume gas density distribution. The effects of the presence of the particulates will be discussed in Section 3.3.2.

More ionization in addition to that occurring in the nozzle was found by the Martin-Marietta Corporation<sup>24</sup> when the region just outside the nozzle was

---

<sup>19</sup>Smith S.D. and A.W. Tatliff, "Rocket Exhaust Plume Computer Program Improvement, Volume IV: Final Report," Report No. LMSC/HREC D162220-IV-A, Lockheed Missiles and Space Company, Huntsville, AL, June 1971.

<sup>20</sup>Penny, M.M., et al., "Supersonic Flow of Chemically Reacting Gas-Particle Mixtures, Volume I: A Theoretical Analysis and Development of the Numerical Solution," Report No. LMSC/HREC TR D496555-I, Lockheed Missiles and Space Company, Huntsville, AL, January 1976.

<sup>21</sup>Penny, M.M., et al., "Supersonic Flow of Chemically Reacting Gas-Particle Mixtures, Volume II: RAMP--A Computer Code for Analysis of Chemically Reacting Gas-Particle Flows," Report No. LMSC/HREC TR D496555-II, Lockheed Missiles and Space Company, Huntsville, AL, January 1976.

<sup>22</sup>Kliegel, J.R. and G.R. Nickerson, "Axisymmetric Two-Phase Perfect Gas Performance Program, Volume I: Engineering and Program Description," Report No. 02784-6006-R000, TRW, 3 April 1967.

<sup>23</sup>"User's Manual for the Two-Dimensional Two-Phase Plume Analysis Computer Program," Report No. SN-141, Dynamic Sciences, Inc., December 1968.

<sup>24</sup>Romine, G.L., et al., "RF Signal Degradation from the MX Stage III Plume," Report No. SE4-116037, Martin-Marietta Corporation, Denver, CO, May 1981.



considered. Presumably, their calculation was done in the region near the thrust axis where the expansion fan from the nozzle tip does not reach until further downstream. However, near the nozzle lip, the expansion is much more rapid and should cause the chemical composition to freeze at the exit value. Thus, downstream of the exit plane, variations of the chemical composition may exist. This aspect of the additional ionization has not been fully investigated and would require additional analysis. At present, we assume the electron mole fraction in the whole plume to be at the nozzle exit value. The electron density anywhere in the plume can then be computed from the gas density distribution. Together with the plume temperature distribution, it enables the collision frequency to be calculated. These are the plasma properties required for determining the interference of the electromagnetic waves by the rocket plume.

### 2.3 RF-PLUME PLASMA INTERACTION

Analysis of the interaction between the RF signals and the plasma is based on the concept of an effective dielectric constant,  $\epsilon_n$ , which depends on the ratios of plasma frequency and collision frequency to the signal frequency.<sup>25</sup>

$$\epsilon_n = \frac{\epsilon}{\epsilon_0} = \left[ 1 - \frac{(\omega_p/\omega)^2}{1+(\nu/\omega)^2} - i \frac{(\omega_p/\omega)^2(\nu/\omega)}{1+(\nu/\omega)^2} \right]$$

where  $\omega = 2\pi f$  is the radian signal frequency,  $\nu$  is the collision frequency for momentum transfer, and the plasma frequency is given by

$$\omega_p = n_e^2 / m_e \epsilon_0$$

---

<sup>25</sup>Heald, M.A. and C.B. Wharton, Plasma Diagnostics with Microwaves, John Wiley & Sons, Inc., New York, NY, p. 6, 1965.

The permittivity of free space is designated by  $\epsilon_0$ , the electron charge by  $e$ , the electron number density by  $n_e$ , and  $m_e$  is the electron mass. A time dependence of  $e^{i\omega t}$  has been assumed.

For a specified signal frequency  $\omega$ , there corresponds a critical electron density  $n_{ec}$  for which  $\omega_p = \omega$ . The plasma is said to be underdense when  $n_e < n_{ec}$  and overdense when  $n_e \geq n_{ec}$ . An overdense medium has a reflective constant of unity so that all signals are reflected and none transmitted through the plasma.

Initial estimates of the effect of the rocket plume on RF propagation from the missile to a ground station were based on ray optics.<sup>26</sup> That is, the incident signal was considered to be a bundle of rays which could be individually traced through the plume. This type of analysis is based on the so-called Eikonal equation<sup>27</sup> which describes the ray trajectories. Absorption of the signal along each ray path can be computed; by comparing the divergence of the incident bundle of rays with that of the existing bundle of rays, the effects of refraction can be determined. The result is that for a given effective radiated power incident on the plasma at some angle, an effective radiated power (ERP) can be computed at a somewhat different exiting angle. Once the transformation from incident to exit angle has been determined, the attenuation of the signal received by a ground station can be obtained by comparing the ERP with and without the plume present. It is possible for an exit angle to correspond to more than one incidence angle, in which case the signals must be summed with the appropriate phasing.

---

<sup>26</sup>Malmud, P., "Raybend--A Tracing Program for Microwaves Propagating through Rocket Plumes," paper presented at the JANNAF 12th Plume Technology Meeting, October 1980.

<sup>27</sup>Born & Wolf, Principles of Optics, Pergamon Press, London, p. 110, 1959.

It has been recognized that the ray optics treatment tends to overpredict the attenuation produced by the plasma plume, especially in the case of large attenuations.<sup>23,29</sup> This is because the analysis is based on the assumption of an infinitesimal wavelength and ignores the signal diffracted around the plume. Early investigators of the RF-plume interaction assumed that the diffraction estimates should be based on a blockage of the incident wave by the overdense core of the plume.<sup>26,27</sup> More recently, it has been noted that a somewhat larger area is blocked, since both the rays incident from the transmitter and rays projected from a ground station are refracted away from the overdense core of the plume.<sup>29</sup> An effective blocked area can be determined by using a ray tracing program and determining the intersection of the rays approaching closest to the overdense core. In these two diffraction estimates, the concentration of the rays at the edge by refraction and the attenuation along the ray path are ignored.

An alternate technique has been developed by Boynton, Davies, Rajasekhar, and Thomson.<sup>30</sup> The effect of the plume is analyzed by dissecting the plasma into a sequence of absorbing phase screens. The incident field is evaluated on a planar surface; the plasma between that plane and the succeeding plane is assumed to modify the field at that plane in phase and amplitude.

Propagation to the next plane is calculated using the Fresnel-Kirchoff integral. Succeeding steps are handled in the same way until the electron density has dropped to a point that phase and amplitude changes are negligible. Fast Fourier transform techniques are used to reduce the computation time. From the Fourier transform of the field at the last plane, the far-field radiation may be directly evaluated. This technique includes, in principle, both refraction and diffraction and has the additional capability that the gross features of plasma turbulence can be included.

---

<sup>28</sup>Vicente, F.A., E.C. Taylor, and R.W. Phelps, "Analysis of Flame Effects in Measured Electromagnetic Propagation Data," J. Spacecraft, 4, pp. 1069-1075, 1967.

<sup>29</sup>Peng, S.Y., "Analytical Model for Predicting R-F Amplitude and Phase Effects of Plume," JANNAF 10th Plume Technology Meeting, 1977.

<sup>30</sup>Boynton, F.W., A.R. Davies, P.S. Rajasckhar, and J.A. Thompson, "Effects of Large Absorbing Rocket Exhaust Plumes on R.F. Signals," JANNAF 10th Plume Technology Meeting, CPI Publications 291, pp. 143-173, 1977.

In this study, we shall first compare the radiated fields from the three different analyses--ray optics, diffraction, and the phase screen approximation --with the computed result for a scattering problem which can be solved exactly. The model will consist of a radially inhomogeneous cylindrical plasma excited by either an electric or magnetic line source. The use of both electric and magnetic line sources will allow the assessment of the effects of the two different polarizations on the result. The plasma parameters will be similar to those computed for the third stage of the MX missile. Although the problem analyzed will be only two-dimensional, it will provide a direct comparison with the results of the diffraction analysis of the MX plume, since that model is also two-dimensional. Comparison will be made with the diffraction model, selecting the strip size based on the assumption of an overdense core or using the ray optics method previously described. Alternate selection procedures will also be considered.

Similarly, the ray optics prediction will be compared with the exact solution to see if there exists any region of validity for its use, particularly at grazing angles to the plume.

Finally, a two-dimensional formulation of the absorbing phase screen model will be compared with the exact solution. Of particular interest will be the manner in which the step sizes must be selected for a given signal frequency and plasma parameters.

It is anticipated that the absorbing phase screen model will provide the best approach to modeling the interaction of the RF with the plasma plume; however, validation of this model is currently unavailable.

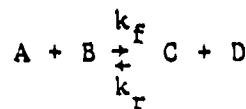
After satisfactory comparison is obtained between the absorbing phase screen model and the exact solution for a cylindrical plasma, an RF-plasma interaction code will be written to use the plasma properties generated by the plume flow field codes in order to compute the effects of the plasma on the phase and amplitude of the RF wave propagating through it.

### 3. RESULTS

In this study, emphasis was placed on examining the sensitivity of the plume density distribution (or, equivalently, the electron density distribution) to various factors in the plume flow field. The aim is to define a theoretical plume flow field model in which all the pertinent phenomena are included. The results of these studies are given below.

#### 3.1 EFFECTS OF IONIC REACTION RATE

As mentioned previously, finite rate chemical reactions must be included in the rocket nozzle flow calculation in order to determine the electron mole fraction at the nozzle exit. Both neutral and ionic reactions need to be considered. The neutral reactions can affect the flow field temperature and the concentrations of the neutral species that enter into ionic reactions. Both have effects on the ionic reaction rate and, therefore, the electron concentration. For a reaction in which the reactants A and B are converted into the products C and D



the specification of the forward reaction rate coefficient  $k_f$  is sufficient, since the reverse rate coefficient  $k_r$  can be computed from the equilibrium constant  $K$ . Thus

$$k_r = k_f / K \quad (1)$$

where  $k_f$  varies with the gas temperature  $T$  as follows:

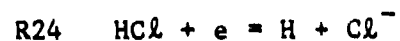
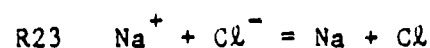
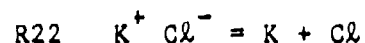
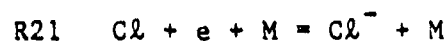
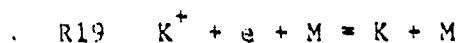
$$k_f = AT^{-n} \exp(-E/RT) \quad (2)$$

where  $R$  is the gas constant and the constants  $n$  and  $E$  are determined from experimental reaction rate data.

For a propellant combination containing the chemical elements C, N, O, H, Cl, Al, K, and Na, the neutral and ionic reactions necessary to describe the chemical system are listed in the Appendix together with the constants in Eq. (2) and their uncertainty limits.<sup>31</sup>

An examination of the reaction rates indicates that large uncertainties exist in their values, especially the ionic reactions which have the dominant effect on the electron concentration. In order to evaluate the uncertainties of the electron concentration in the plume due to the inaccuracies of the reaction rates, the electron mole fraction at the nozzle exit plane was calculated for the nominal value and the upper and lower bounds of the ionic reaction rates as listed in Table 1 and the Appendix. The results are listed in Table 2 for a solid propellant containing 80 ppm sodium and 30 ppm potassium.

Table 1. Ionic Reactions




---

<sup>31</sup>Jensen, D.E. and G.A. Jones, "Gas-Phase Reaction Rate Coefficients for Rocketry Applications," Rocket Propulsion Establishment Report No. 71/9, Ministry of Defense, London W.C. 2, October 1971.

Table 2. Effects of Ionic Reaction Rates on Electron Mole Fraction at Nozzle Exit

Reaction Rate	Electron Mole Fraction
Nominal	$3.6 \times 10^{-7}$
5 x R19 and R20	$6.27 \times 10^{-7}$
1/5 x R19 and R20	$1.13 \times 10^{-6}$
30 x R21	$9.2 \times 10^{-7}$
1/30 x R21	$7.45 \times 10^{-7}$
10 x R22 and R23	$8.46 \times 10^{-7}$
1/100 x R22 and R23	$5.38 \times 10^{-7}$
30 x R24	$2.8 \times 10^{-6}$
1/100 x R24	$3.86 \times 10^{-7}$

It appears that no significant change in the electron density is caused by the uncertainties in the first five reactions. The two-body attachment reaction (Reaction 24), however, has the predominant effect on the ionization level as shown in Table 2 and Fig. 1 where  $X_e$  denotes the electron mole fraction,  $R^*$  the throat radius, and  $Z$  the axial distance from the throat. The uncertainties in its reaction rate can cause a factor of three increase or a factor of two decrease in the electron density from the value predicted on the basis of its nominal rate. Therefore, based upon the state of the art in the reaction rates, an uncertainty factor of about seven in the plume electron density is to be expected.

This situation will prevail until such time that the rate of Reaction 24 can be more accurately determined by laboratory experiment. In the absence of more accurate reaction rate data, the recommended approach is to vary the rate of Reaction 24 to match existing flight data, such as some of the S-band telemetry data available for Minuteman Stage III flights from Vandenberg. The same reaction rate is then used to predict plume effects on RF signals for future flights.

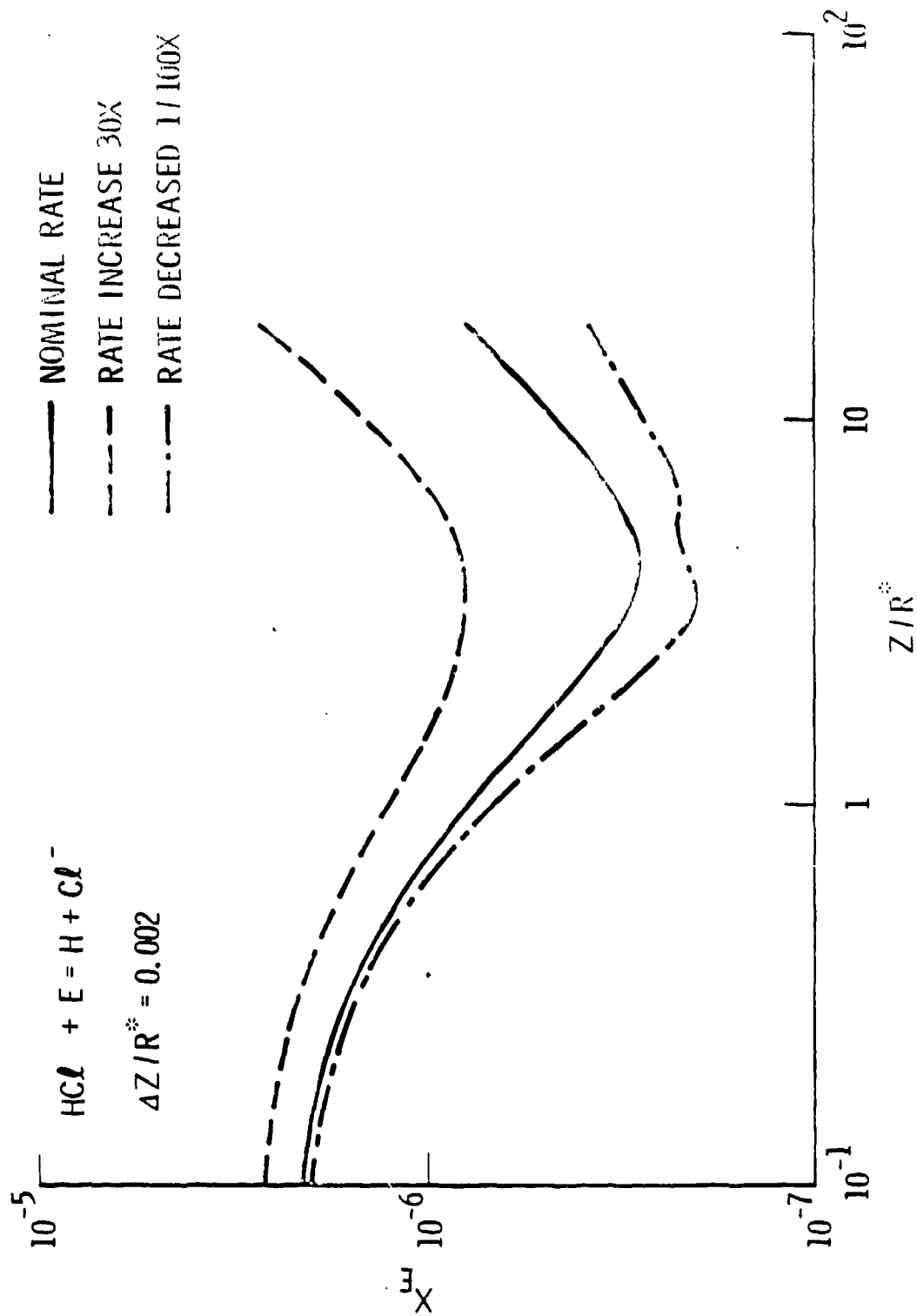


Fig. 1. Effect of Two-Body Electron Attachment Rate



The dominant effect of Reaction 24 can be traced to the fact that in the nozzle the gas density is rapidly decreasing. Since the rate of Reaction 24 is proportional to the density square while those of Reactions 19 to 21 are proportional to the density cube, the flow expansion in the nozzle causes the Reactions 19 through 21 to slow down much more. Reaction 24 obviously proceeds in the reverse direction in the nozzle to generate more electrons from the negative chlorine ion. Since the concentration of atomic hydrogen is orders of magnitude higher than the other reactants in Reactions 19 to 23, an uncertainty in the rate of Reaction 24 produces much greater error in the electron density. This is illustrated in Figs. 2 and 3 where the species from a solid propellant exhaust are plotted. This propellant contains a low percentage of ammonium perchlorate so that the amount of  $\text{HCl}$  formed is only 1 percent by mole. Also  $\text{Al}^+$  exists in the nozzle but was not included in Fig. 3. The major species ( $\text{CO}$ ,  $\text{H}_2$ ,  $\text{H}_2\text{O}$ ,  $\text{CO}_2$ , and  $\text{HCl}$ ) are essentially frozen during the flow expansion in the nozzle. However, the minor neutral species and the ionic species undergo considerable change. This demonstrates the importance of accounting for finite rate chemical reactions in the nozzle when ionization of the rocket engine exhaust is considered. The ionization reactions are so fast that considerable care must be exercised in choosing a sufficiently small integration step size to integrate the species conservation equations. It was discovered that by reducing the integration step size progressively, the solution no longer changed when a step size equal to or less than 0.2 percent of the throat radius was taken. This is shown in Fig. 4 together with a solution using a step size equal to 1 percent of the throat radius. Clearly, large errors can result when the integration step size is too large. A step size of  $\Delta z/R^* = 0.002$  was adopted for all chemical kinetic calculations in this study.

### 3.2 TWO-PHASE FLOW IN ROCKET NOZZLE

Liquid propellants generally do not form condensed solid particles except perhaps from erosion of the nozzle throat. In that case, the amount of particulates carried by the exhaust gas is so small that effects on the flow field can be neglected.

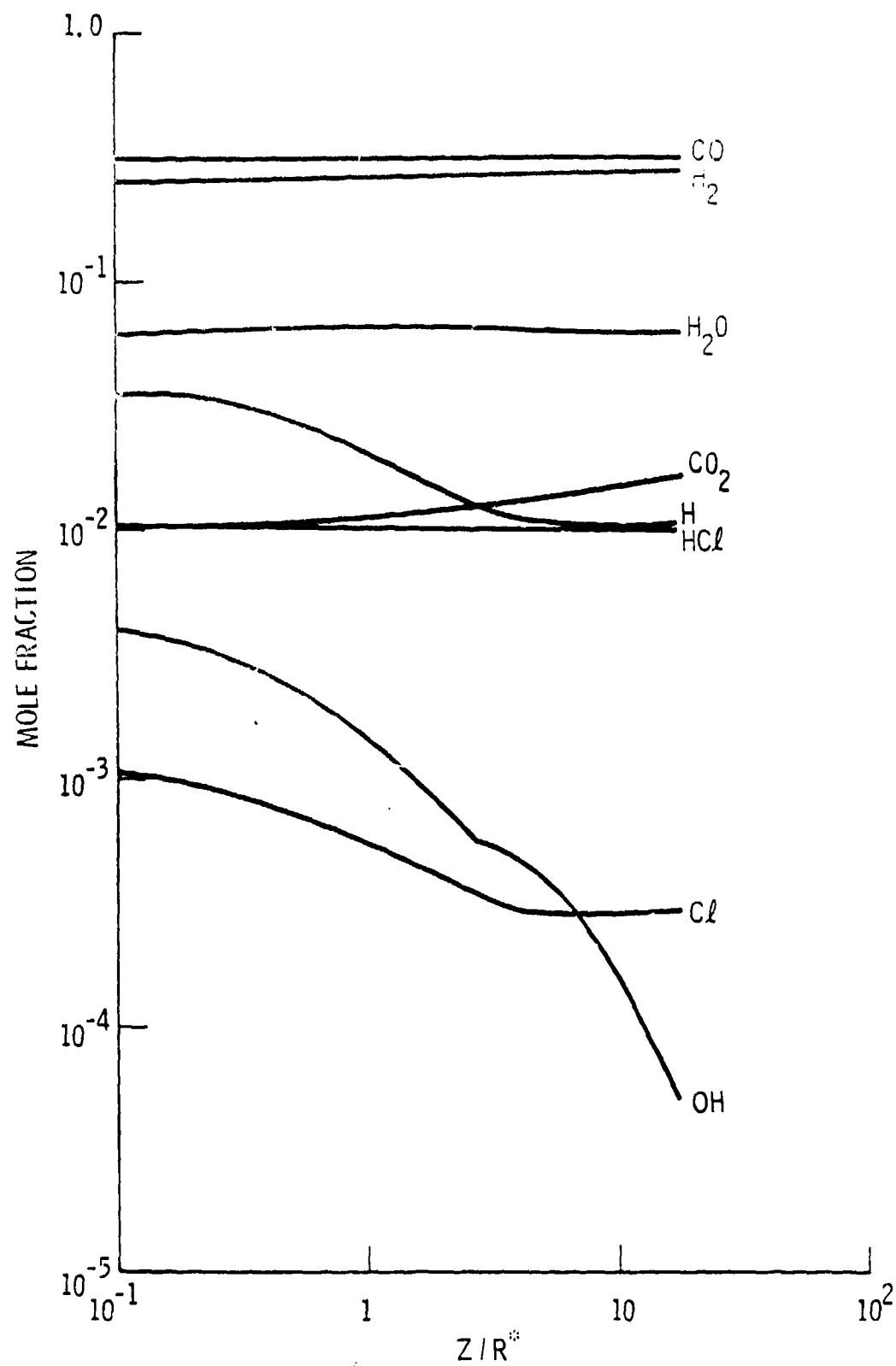


Fig. 2. Neutral Chemical Species Distribution along Rocket Nozzle (composite double-based)

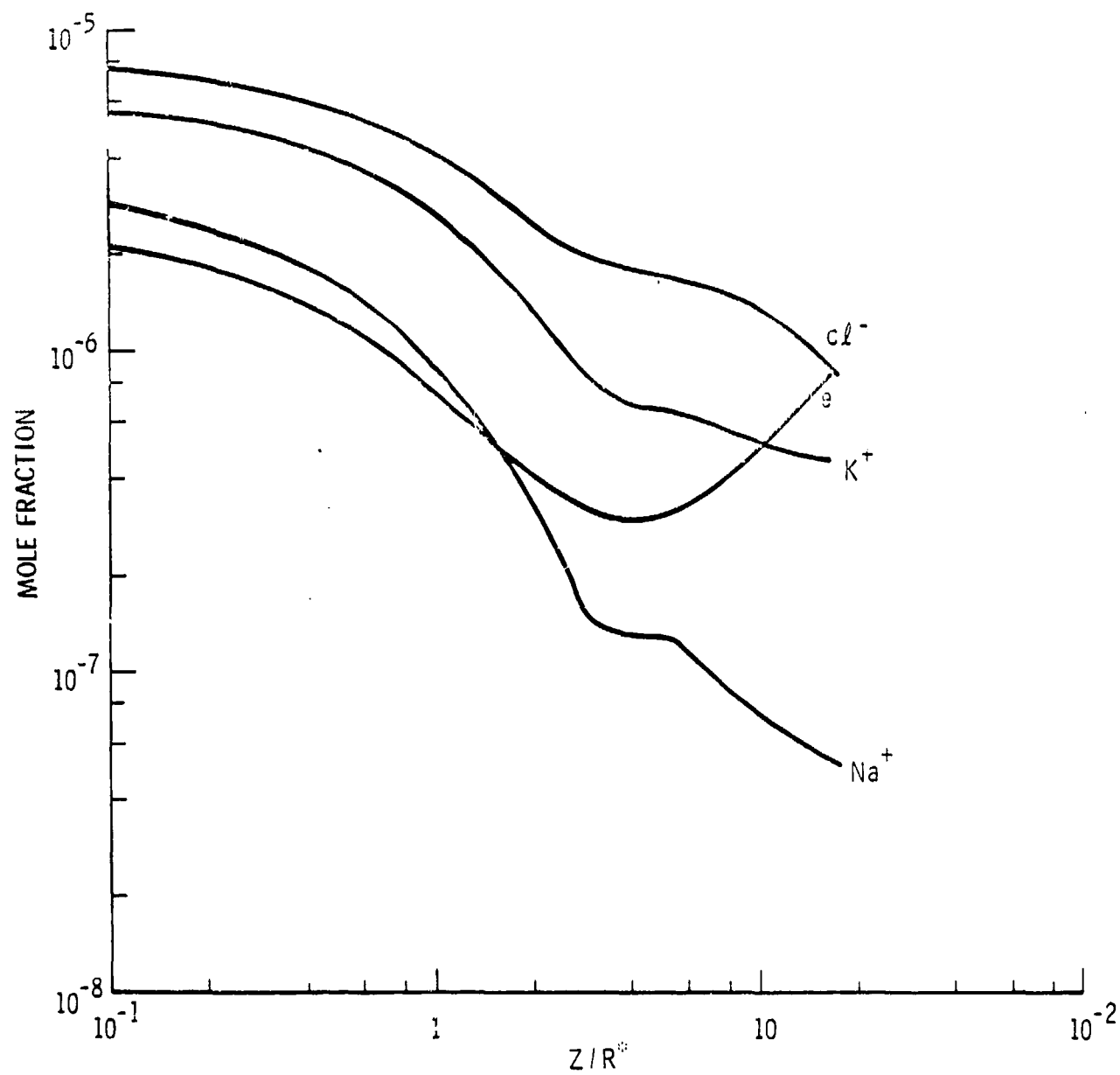


Fig. 3. Ionic Species Distribution along Rocket Nozzle

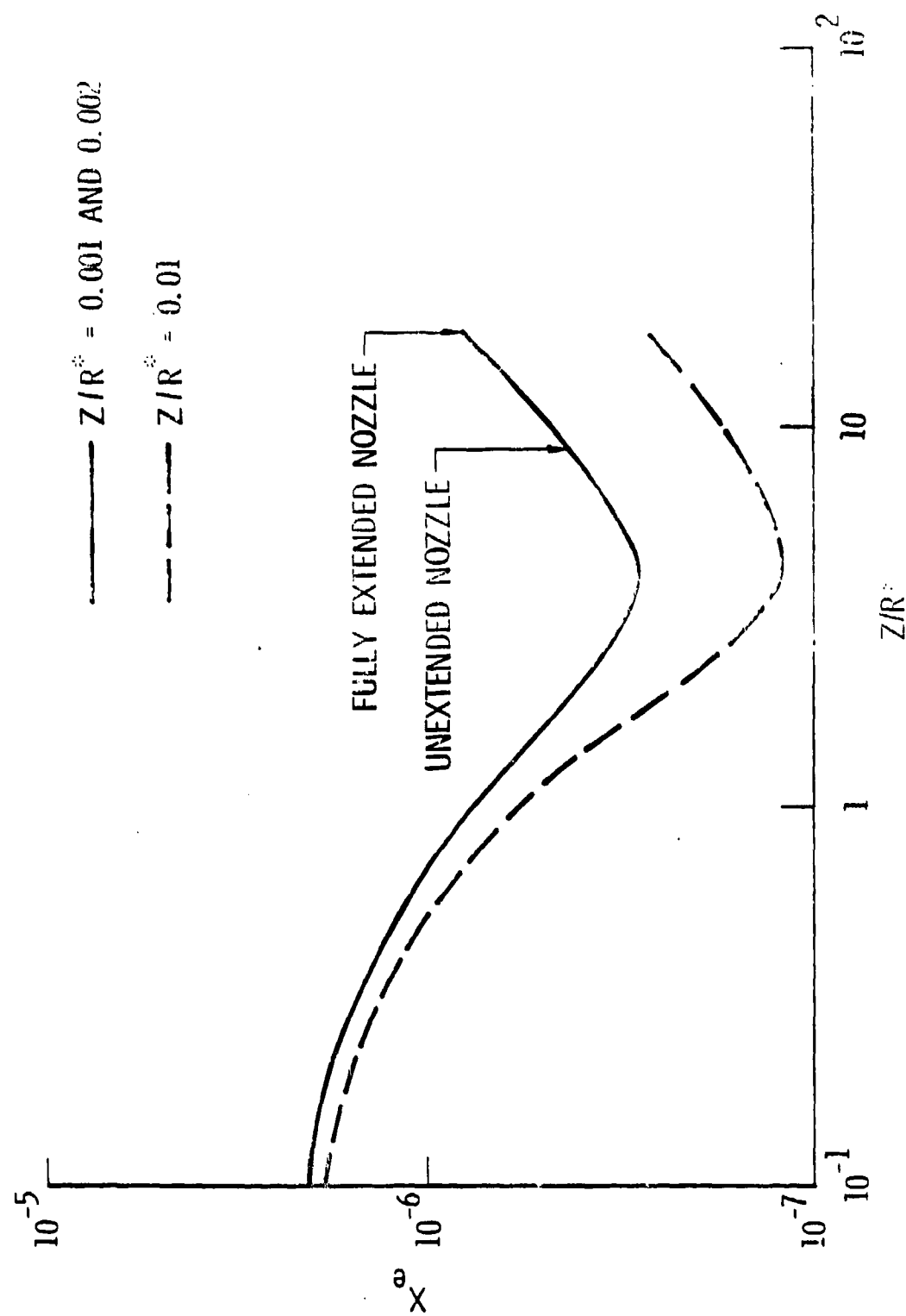


Fig. 4. Effect of Integration Step Size on Electron Mole Fraction

Solid propellants generally contain aluminum as part of the fuel. As the propellant burns, the aluminum is oxidized, forming liquid aluminum oxide particles of various sizes and other gaseous aluminum compounds. The liquid droplets solidify into solid particles when they cool to the melting point of aluminum oxide by losing heat to the expanding gas in the nozzle. The amount of particulates formed can be a large fraction of the total exhaust, generally from 20 to 40 percent, depending upon the propellant formulation.

The presence of large amounts of particulates in the rocket nozzle causes considerable momentum and heat transfer between the gas and the particles. A fully coupled two-phase flow solution was obtained for the MX third stage nozzle geometry, using the Aerospace CY3D2P code. Perfect gas and single size particles of 6.7  $\mu\text{m}$  diameter were assumed. Table 3 lists the gas and solid properties used in the calculation.

Table 3. Gas and Solid Properties for Two-Phase Nozzle Flow Calculation

Gas Phase	Particle Phase
Ratio of specific heats = 1.318	Particle diameter = 6.7 $\mu\text{m}$
Heat capacity = 0.436 Btu/lb-°R	Particle heat capacity = 0.326 Btu/lb-°R
Prandtl number = 0.5	Solid mass density = 200 lb/ft <sup>3</sup>
Emissivity = 0.0	Emissivity = 0.25
Chamber pressure = 693 psia	Percentage by weight of particles = 30.5%
Chamber temperature = 6000°R	
Viscosity at 6000°R = $5.67 \times 10^{-5}$ lb/ft-sec	
Temperature exponent for viscosity = 0.65	

Figure 5 shows the MX third stage motor configuration and the domain used in the transonic analysis. The expanded view of this domain and the grid system for the computation are shown in Fig. 6. At the left side of the transonic domain, the gas is subsonic. It attains sonic velocity in the throat region and passes through the right-hand computational boundary supersonically. In the transonic domain, the unsteady two-phase governing equations are solved by finite differences to avoid the difficulty of having to solve mixed elliptical-hyperbolic differential equations. The computation marches in time until the flow variables no longer change in time and the solution reaches steady state. The solution is continued into the expanding nozzle until the nozzle exit is reached. In this region, the steady-state governing equations are solved. The computational grids at a number of selected axial stations are depicted in Fig. 7.

The results of the computation with and without the particles are shown in Figs. 8 through 15 to demonstrate the effects of the particles on the nozzle flow. Contours of constant Mach number and ratio of gas density to chamber density from the two-phase flow solution are plotted in Figs. 8 through 11. The large radial gradient of the Mach number near the nozzle wall as shown in Fig. 8 is the result of the absence of the particulates. The particles cannot negotiate the large throat curvature, and a limiting particle streamline is formed. At nozzle radius larger than the boundary of this limiting streamline, the region is occupied only by the gas.

Similar contour plots from the solution without the particles are presented in Figs. 12 through 15. Comparison of the results with and without the particles shows that the presence of the particles greatly decreases the gas Mach number, while the gas density is relatively unaffected.

In order to check the validity of the SPP code, the same case was computed using identical gas and particle properties and the perfect gas mode of the SPP code. Radial profiles of gas properties at the nozzle exit plane are compared with those obtained from the Aerospace CY3D2P code in Figs. 16 and 17. Satisfactory agreement of the results from the two codes is obtained for Mach

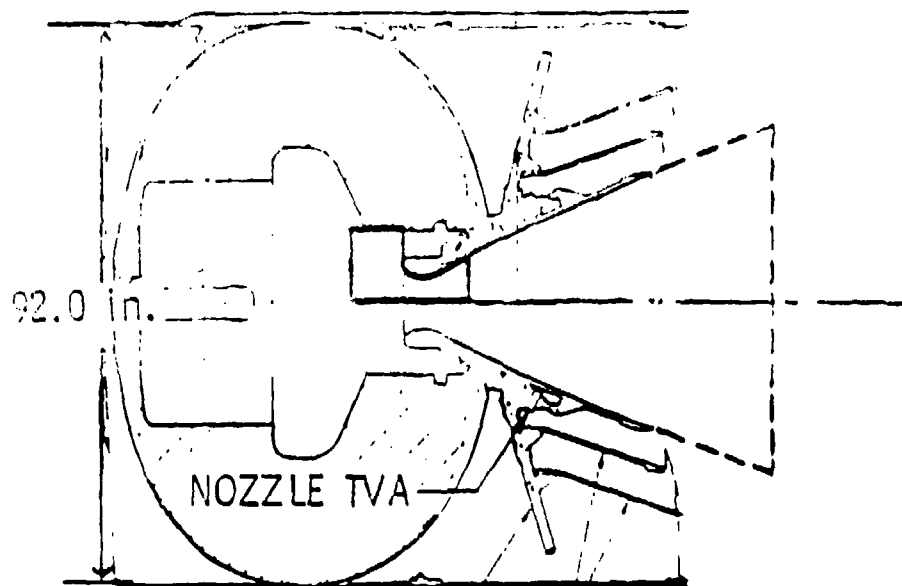


Fig. 5. MX Third Stage Motor Interior Configuration

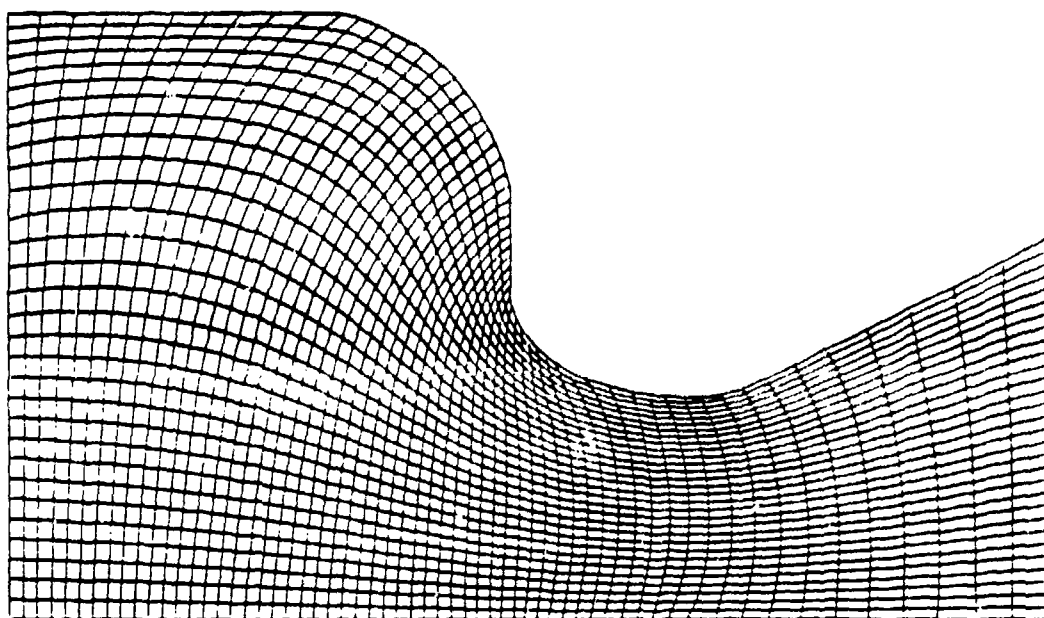


Fig. 6. Computational Grid for Transonic Flow Regime

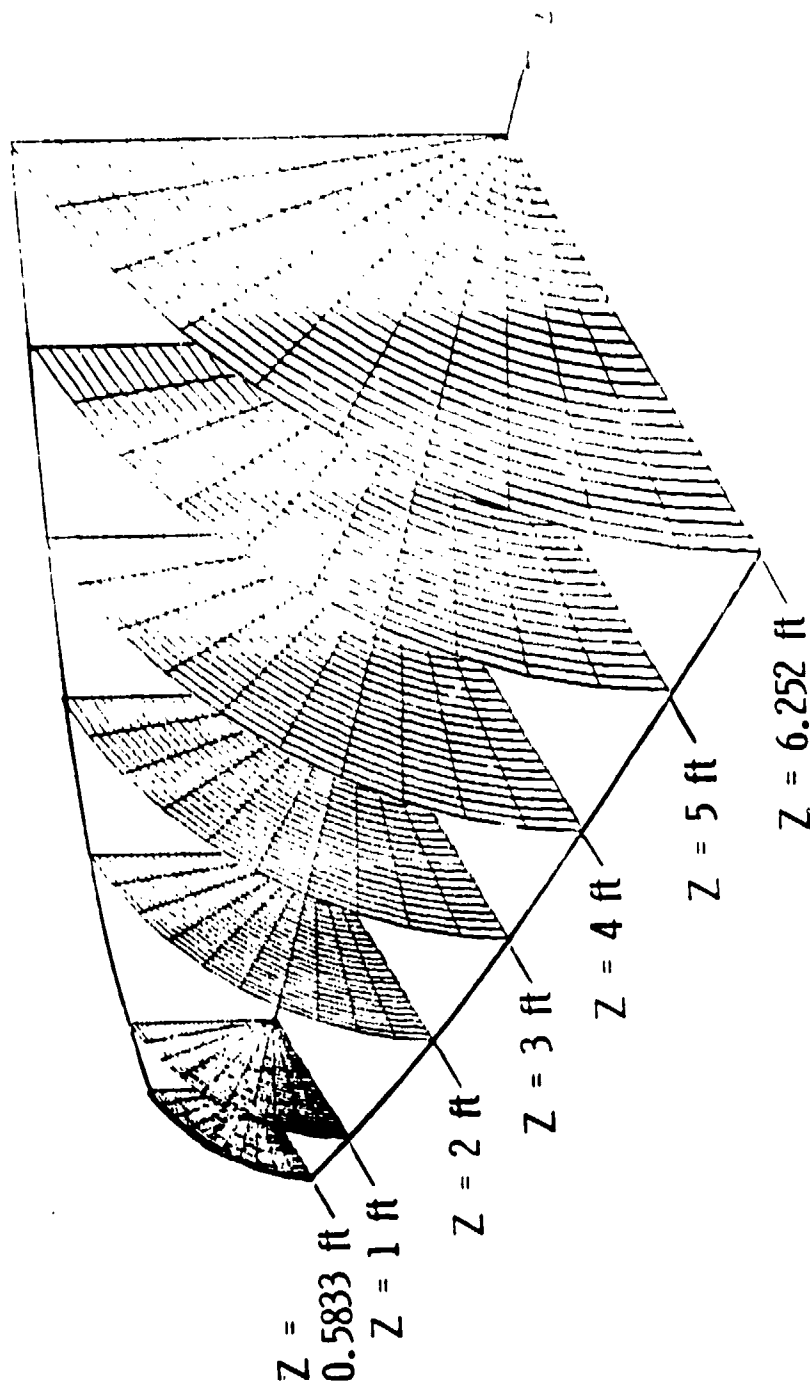


Fig. 7. Cross-Sectional Grid for Supersonic Flow Region



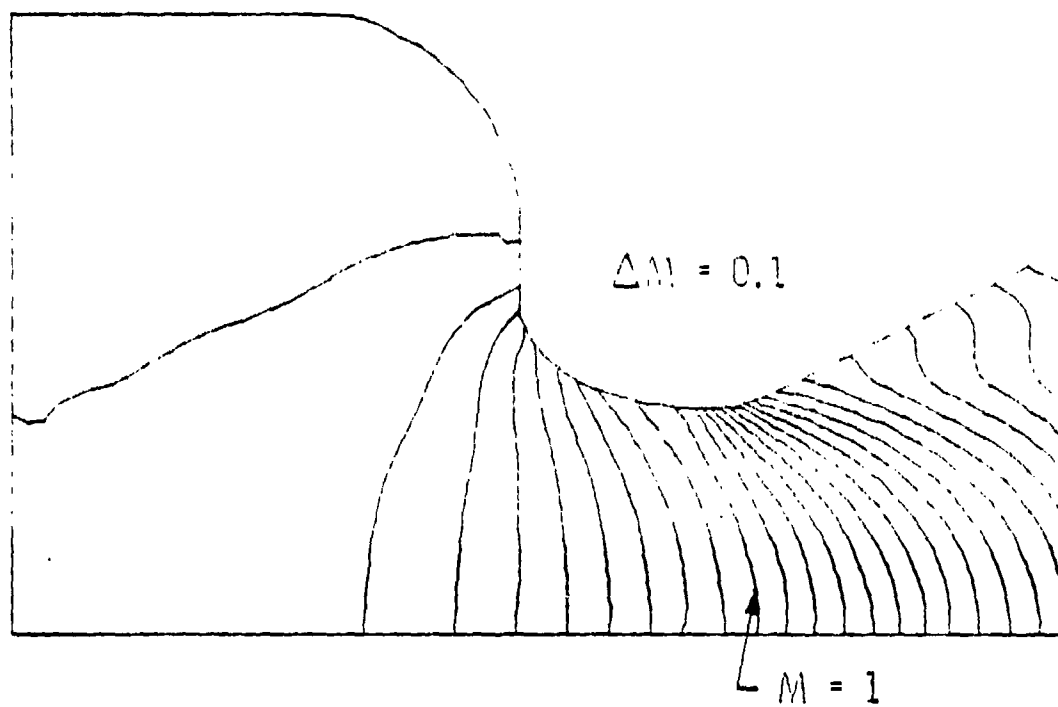


Fig. 8. Mach Number Contour, Two-Phase  
(Transonic Regime)

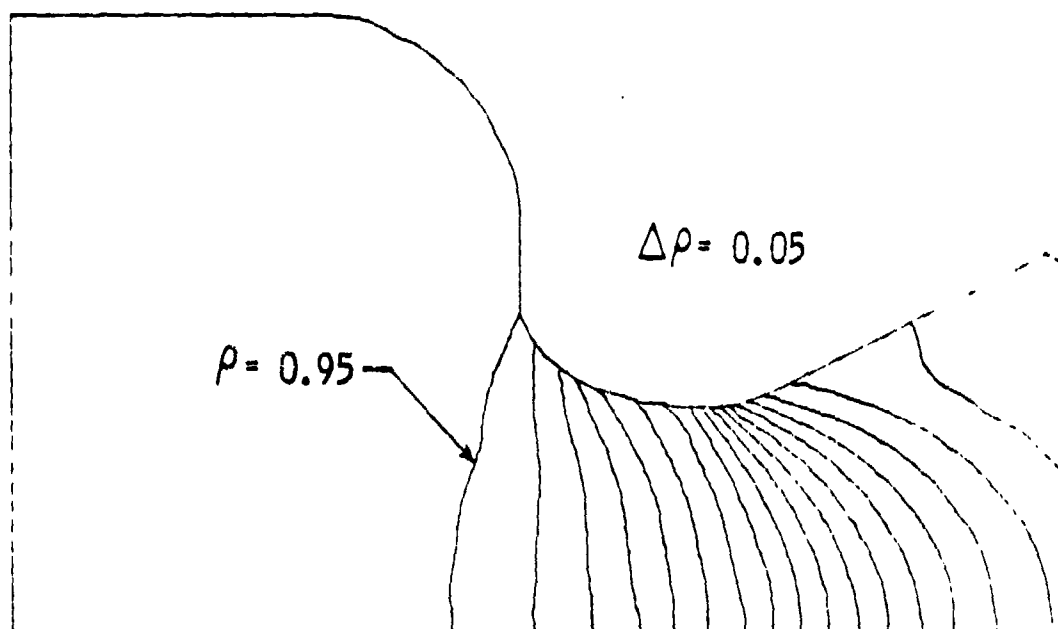


Fig. 9. Gas Density Contour, Two-Phase  
(Transonic Regime)

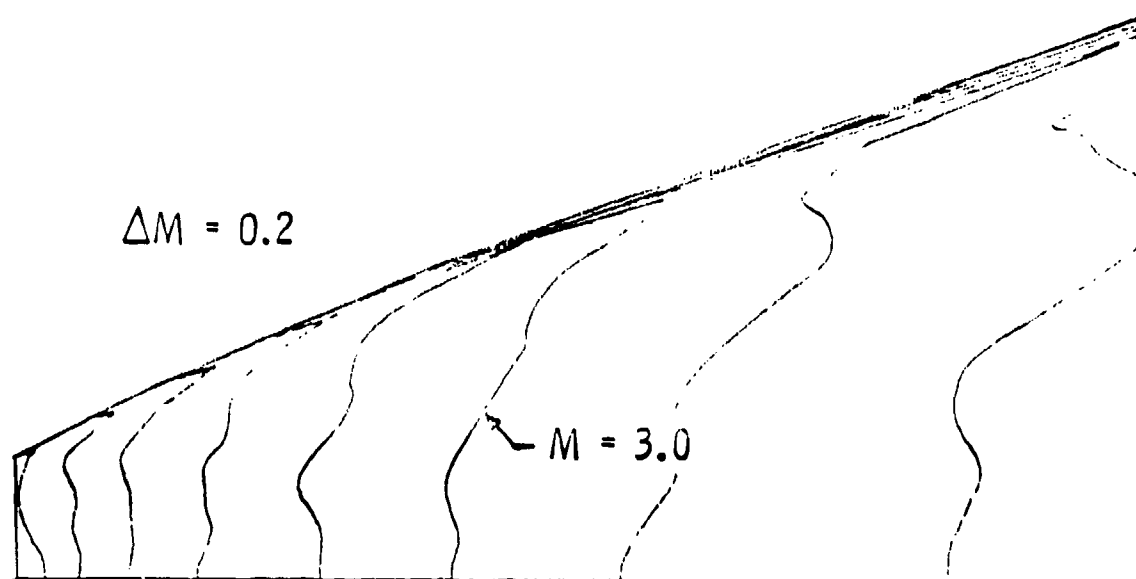


Fig. 10. Mach Number Contour, Two-Phase  
(Supersonic Regime)

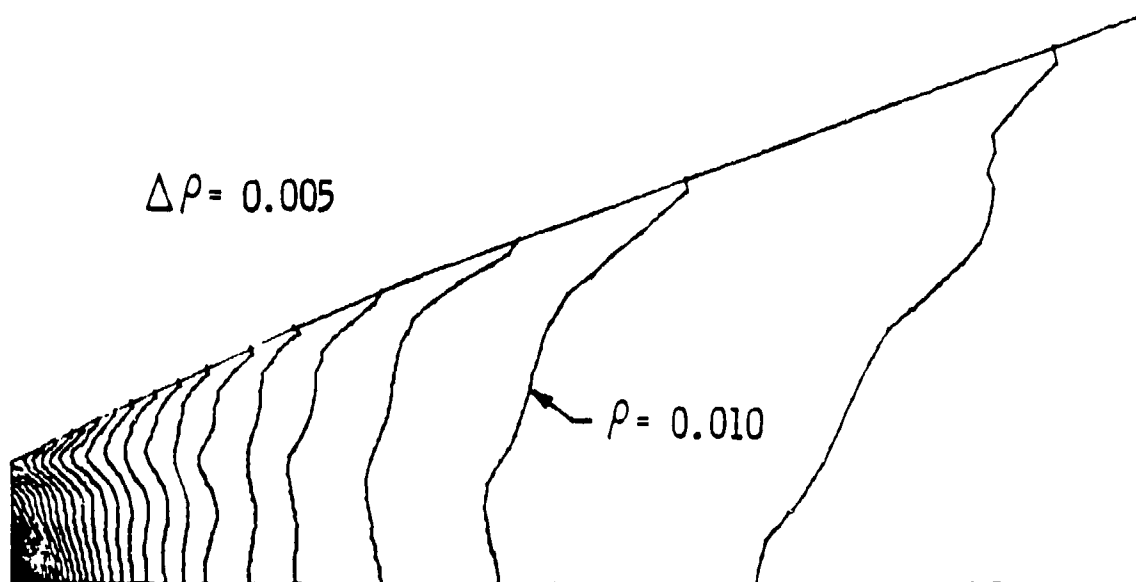


Fig. 11. Gas Density Contour, Two-Phase  
(Supersonic Regime)

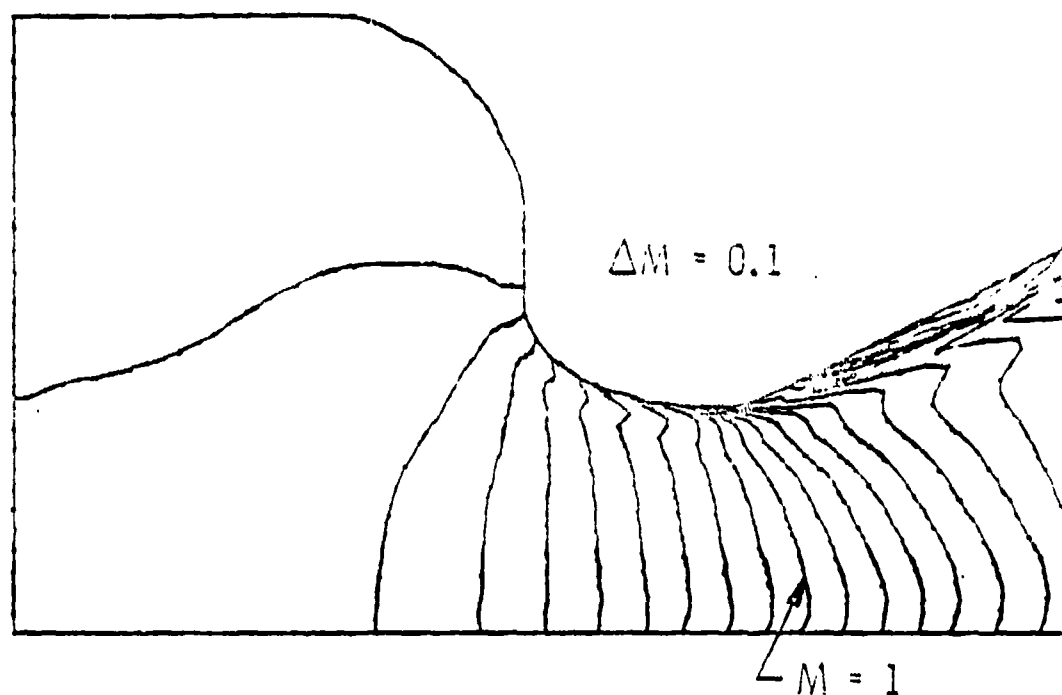


Fig. 12. Mach Number Contour, One-Phase  
(Transonic Regime)

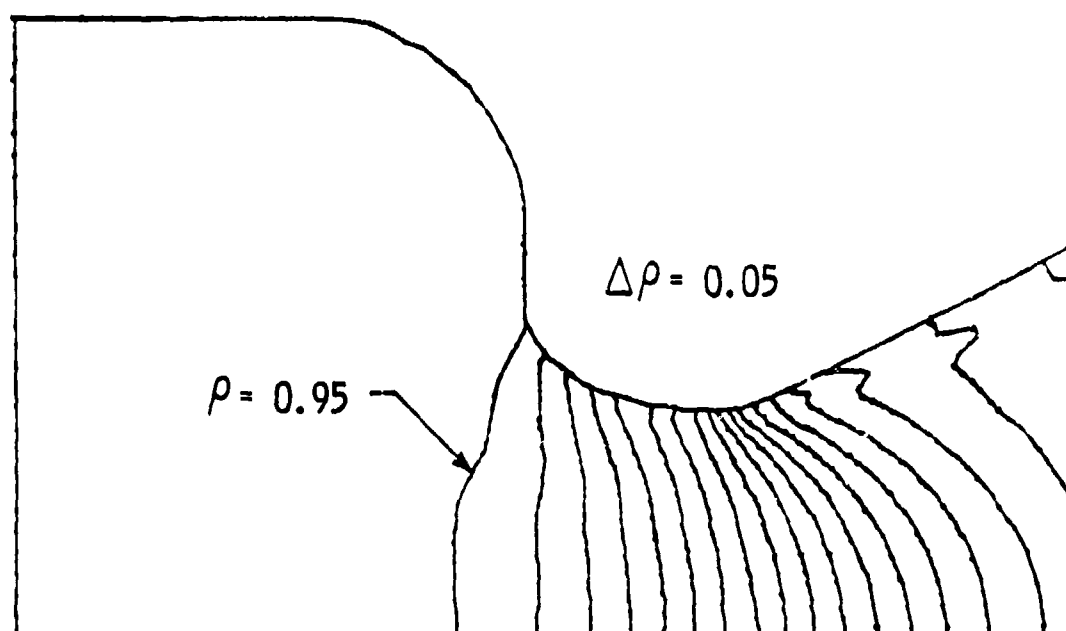


Fig. 13. Gas Density Contour, One-Phase  
(Transonic Regime)

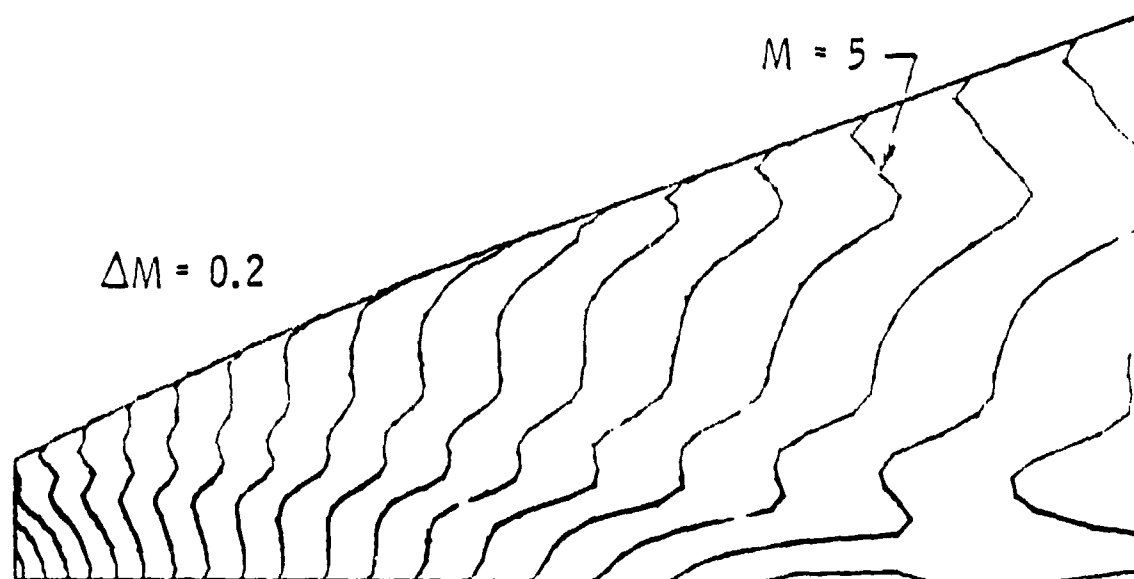


Fig. 14. Mach Number Contour, One-Phase  
(Supersonic Regime)

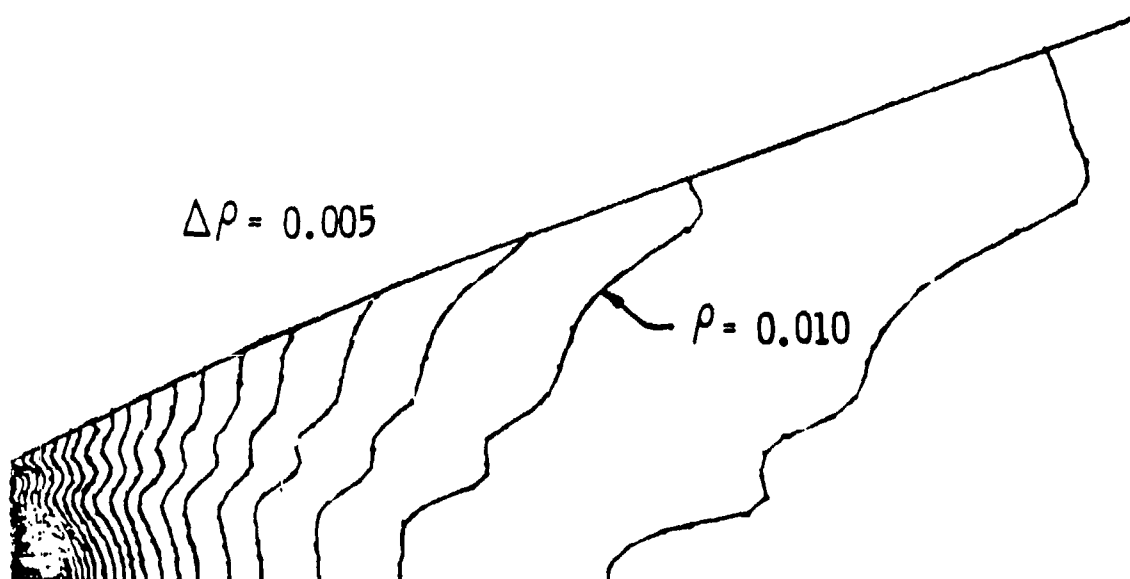


Fig. 15. Gas Density Contour, One-Phase  
(Supersonic Regime)

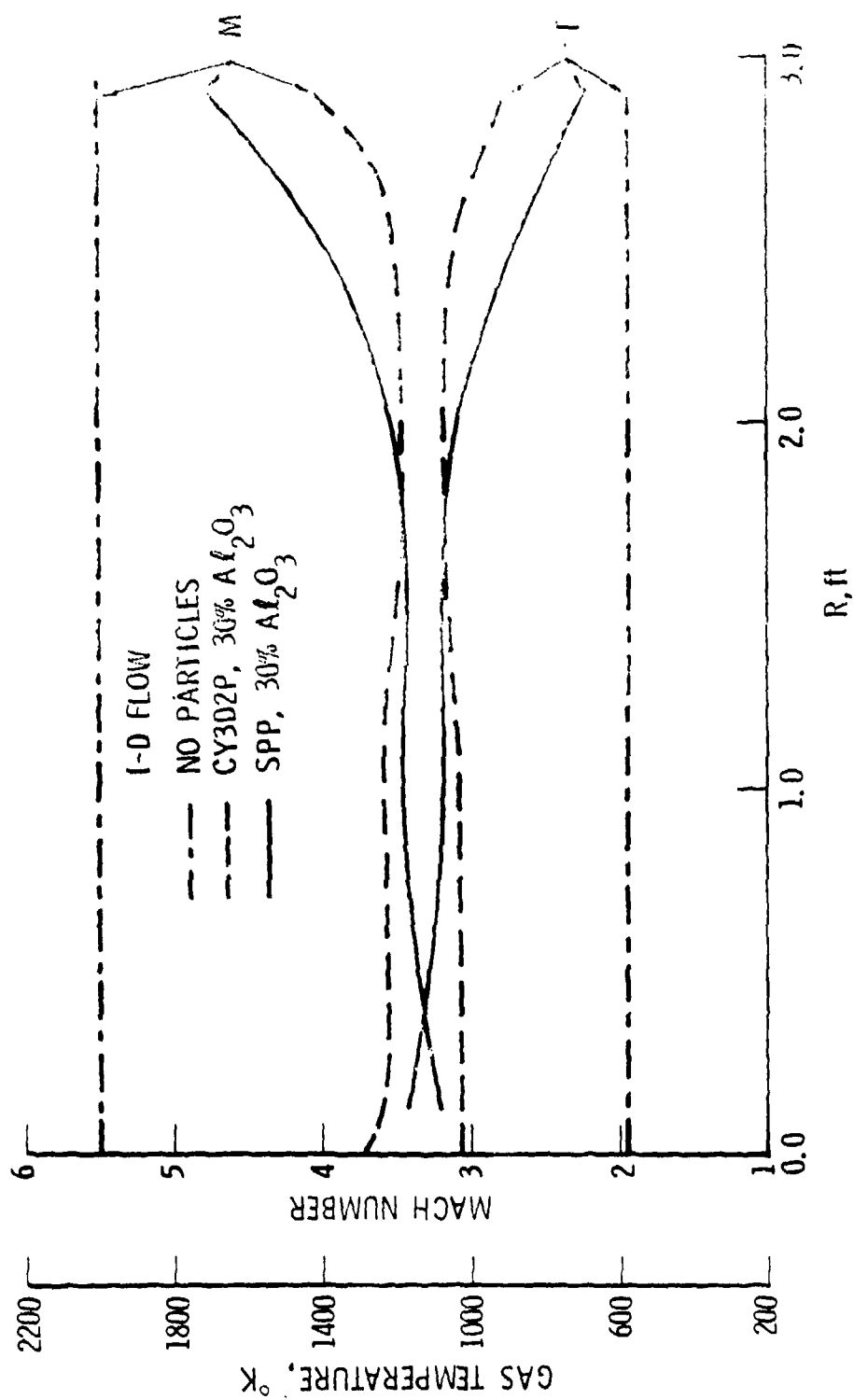


Fig. 16. Profiles of Mach Number and Temperature at Nozzle Exit Plane with Single Particle Size of 6.7  $\mu m$

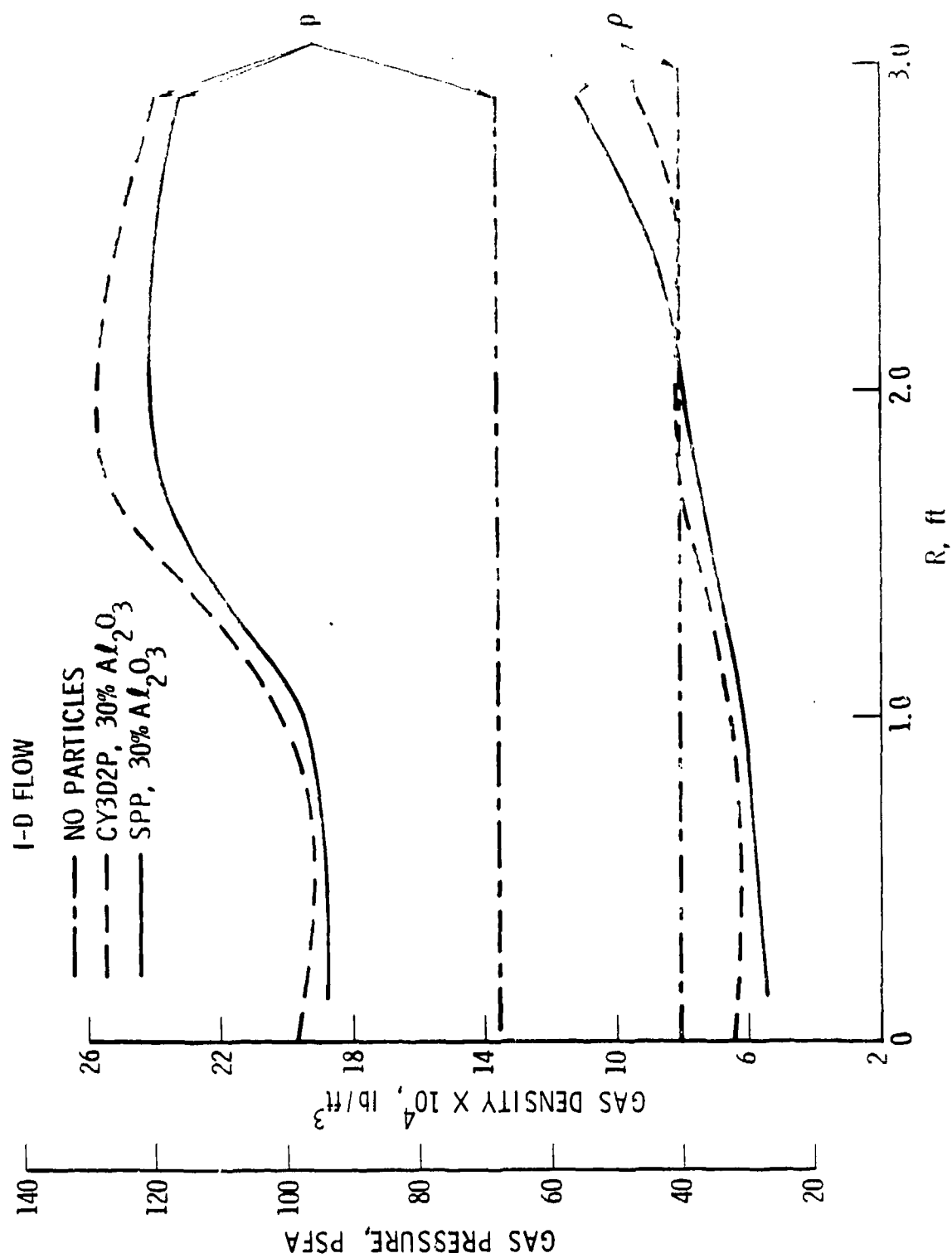


Fig. 17. Profiles of Pressure and Density at Nozzle Exit Plane with Single Particle Size of 6.7  $\mu$ m

number, temperature, pressure, and density. The small differences can be explained in part by the different particle drag and heat transfer coefficients adopted by the two codes. It is interesting to note that the gas temperature is about 400°K higher when particles are present. The particles, cooling at a lower rate, heat up the gas. As a result, the gas temperature is increased in the core. The particles are absent near the nozzle wall, and the gas temperature starts to approach the value for one-dimensional gas flow without particles. The lowering of the Mach number in the two-phase flow is largely due to the higher gas temperature as the sonic velocity is greater.

With the SPP code validated for the case of a single-size particle, two-phase flow computation for a distribution of particle sizes was made. For a 4.32-in. throat radius of the MX third stage, the SPP code predicts a mean particle diameter of 6.7  $\mu\text{m}$ . A log normal distribution is then assumed to divide the particles into five diameters of equal weight, viz., 3.01, 4.89, 6.34, 9.56, and 15.6  $\mu\text{m}$ . Figure 18 shows the gas temperature and density profiles at the nozzle exit plane. The gas temperature increase in the core is again seen when particles are present. The radial temperature gradient is much steeper in Fig. 18 than that shown in Fig. 16. This is due to the multiple particle sizes. The drag-to-weight ratio of the particles is smaller as the particle diameter is increased. Consequently, the gas cannot turn the larger particles sufficiently to reach the nozzle lip. The larger particles, therefore, remain in the core. The limiting streamline locations shown in Fig. 18 for the various particle sizes define the largest radial location in the nozzle such particles can extend. Thus, more particles are located closer to the nozzle axis and cause more heating of the gas. The shape of the gas temperature profile is the result of this separation of particle sizes.

These results for the case of multiple particle sizes differ from those of single-size particles not only because of the particle size effect but also because of the differences in the chamber condition and the gas properties in the two computations.

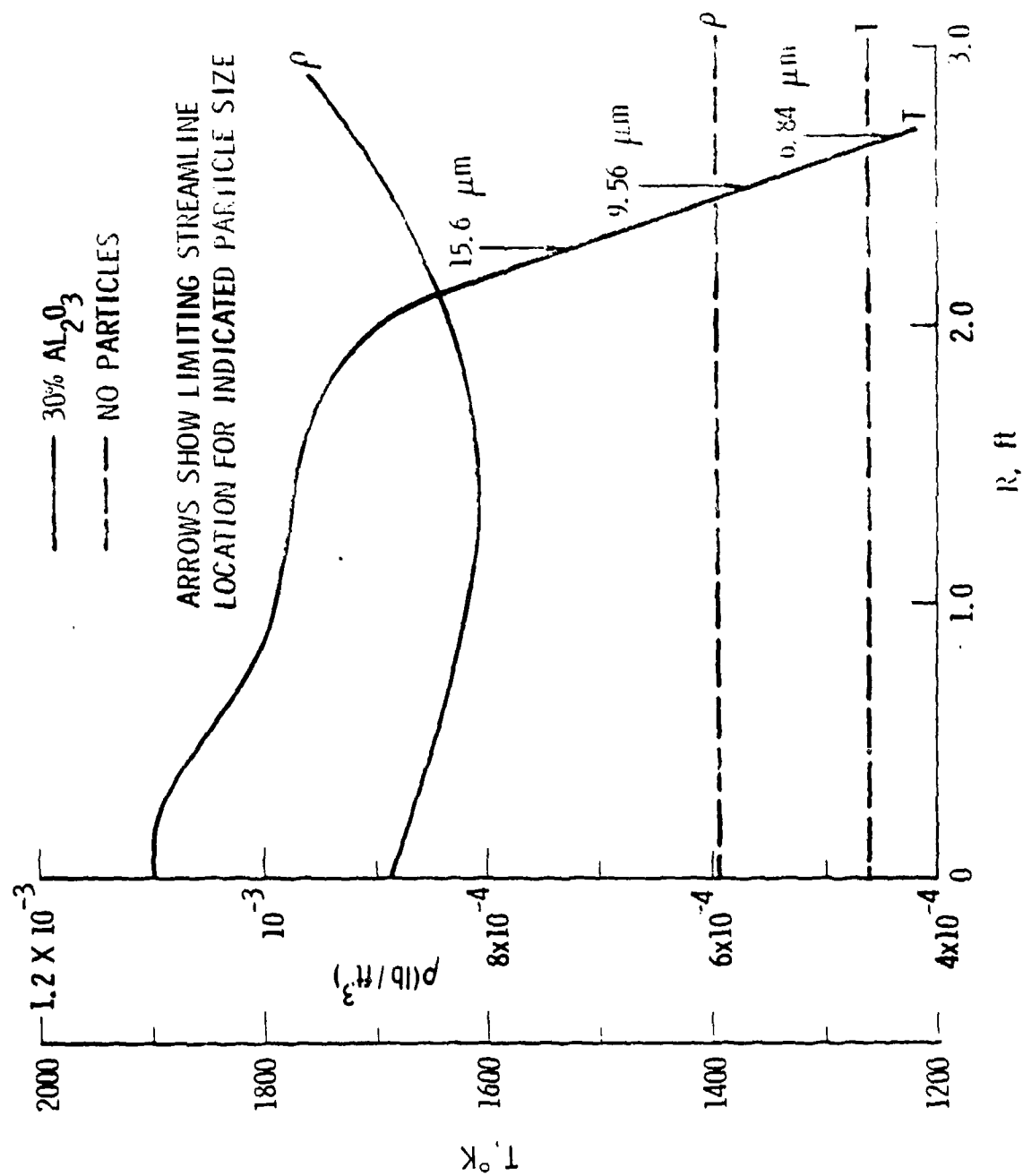


Fig. 18. Radial Profiles of Gas Temperature and Density at Nozzle Exit



Figure 19 shows the Mach number  $M$  and pressure  $p$  variation across the nozzle exit. The lowering of the Mach number in the core is undoubtedly related to the higher gas temperatures. However, the gas also loses considerable momentum in accelerating the particulates as shown by the product  $(1/2)\rho p M^2$ , the gas momentum flux.

The mechanisms for creating particles of various sizes are complex and not well understood. The combustion process undoubtedly plays a part. It was discovered, however, that the mean particle size is somewhat dependent upon the throat radius. As the particles travel through the throat region, they are still in a molten form. The shear force in the throat region causes the particles to break up into smaller sizes. Some correlation of experimental data does show the mean particle size to increase with the throat radius (less shear forces). A correlation by Radke, et al.<sup>32</sup> yields 9  $\mu\text{m}$  mean particle diameter for the nozzle throat radius of the MX third stage engine. In order to determine the sensitivity of the particle sizes, the two-phase nozzle flow analysis was repeated for the increase in the mean particle diameter from 6.7  $\mu\text{m}$  to 9  $\mu\text{m}$ . Comparison of the exit Mach number profiles in Fig. 20 shows that the uncertainty in the particle size does not introduce large deviations in the gas flow properties, unless the mean particle diameter is grossly in error.

We have shown that the presence of the particulates in the nozzle causes appreciable changes in the gas properties at the nozzle exit plane. This will subsequently affect the gas density (and electron density) in the exhaust plume, the extent of which will be discussed in Section 3.3.2.

---

<sup>32</sup>Radke, H.H., L.J. Delaney, and P. Smith, "Exhaust Particle Size Data from Small and Large Solid Rocket Motors," Report No. TOR-1001(S2951-18)-3, The Aerospace Corporation, El Segundo, CA, July 1967.

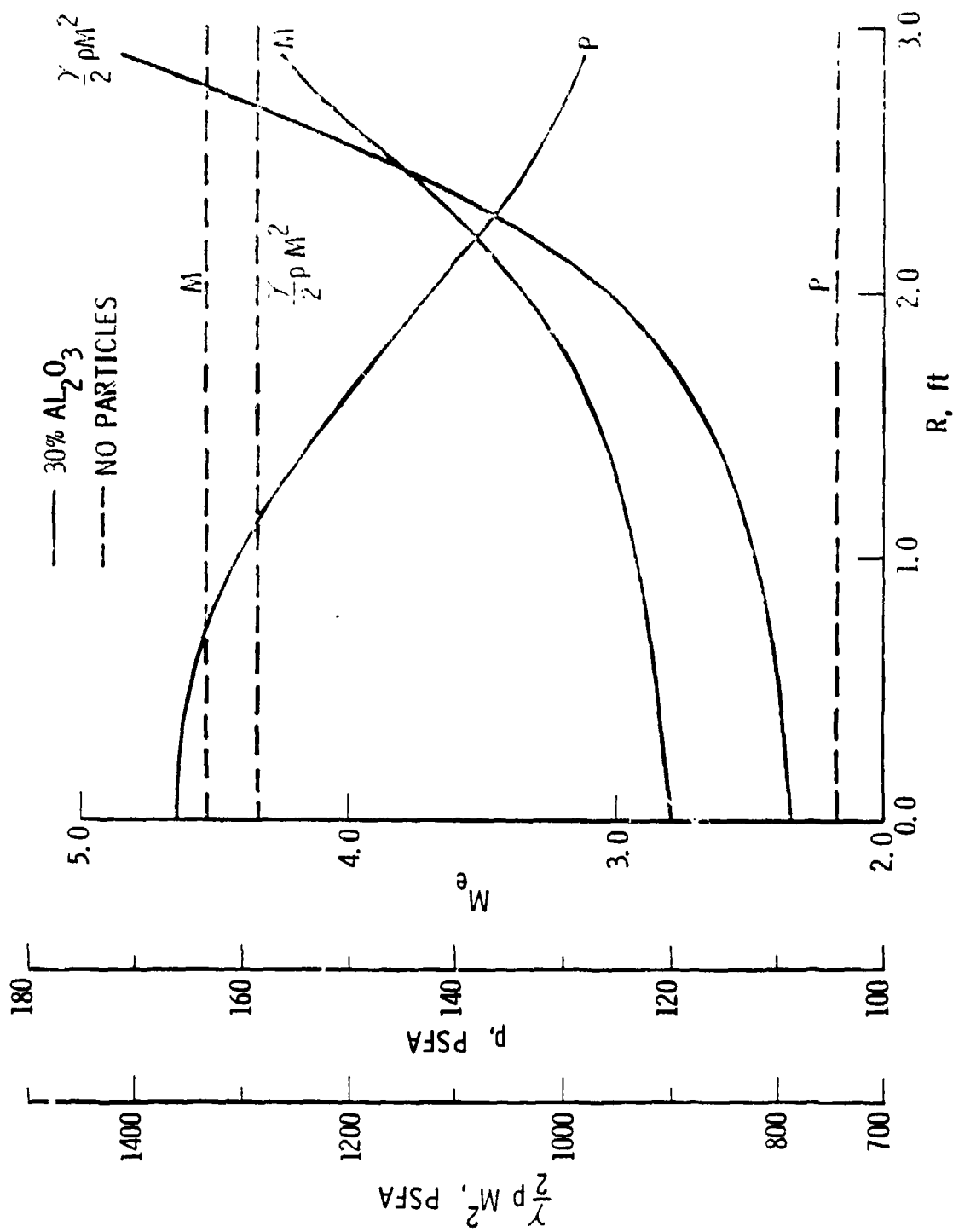


Fig. 19. Radial Profiles of Mach Number and Gas Pressure at Nozzle Exit

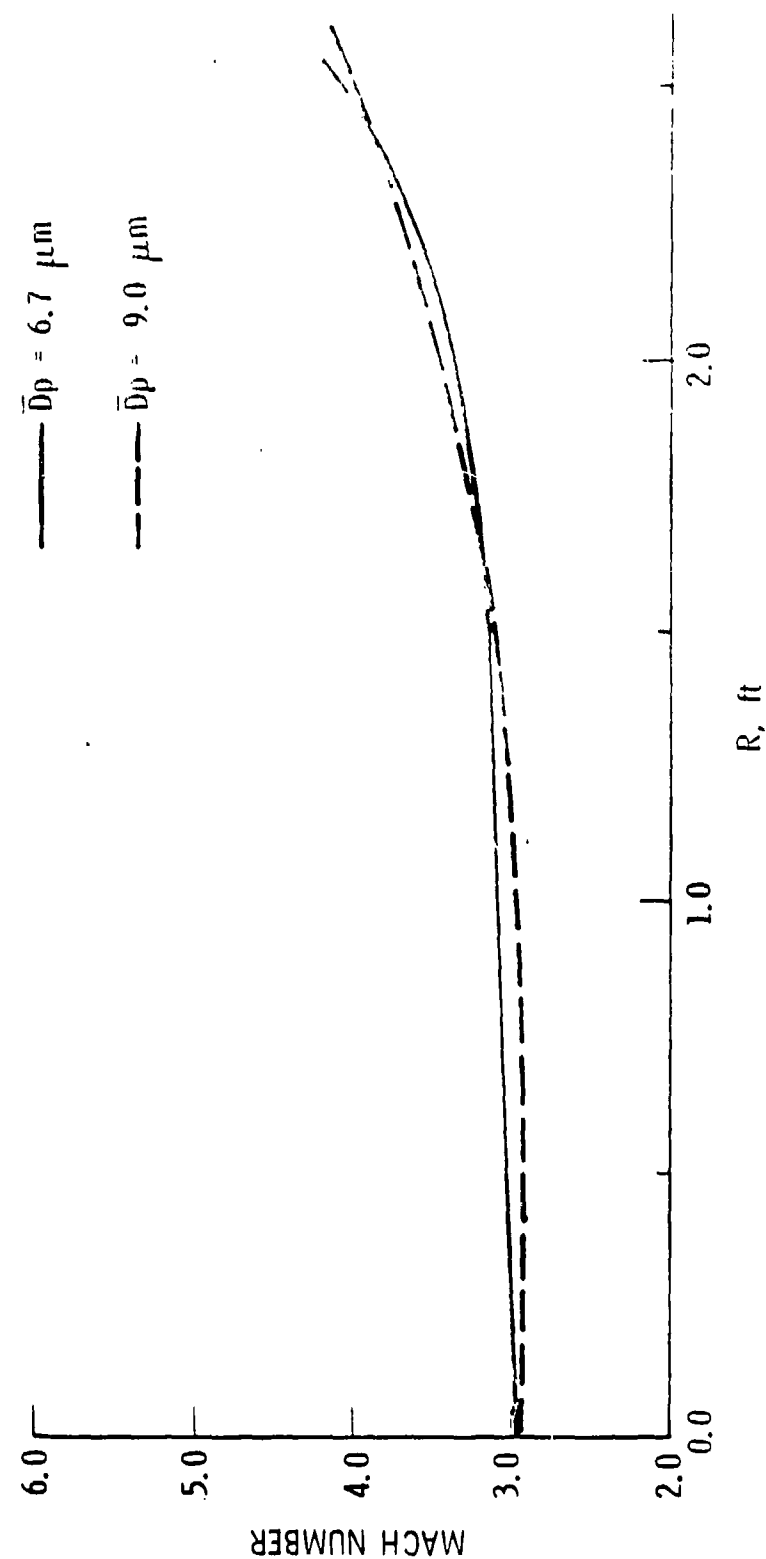


Fig. 20. Effect of Mean Particle Diameter on Exit Mach Number

### 3.3 ROCKET EXHAUST PLUME FLOW FIELD

With the flow properties determined at the nozzle exit plane, the computation can then proceed into the exhaust plume. At very high altitudes, where the atmosphere is very thin, the rocket exhaust can be assumed to expand into a vacuum and the gas density decrease monotonically with increasing distance from the nozzle and with increasing polar angle from the plume centerline. At lower altitudes, however, interaction between the atmosphere and the plume gas confines the plume into a region the boundary of which is determined by a balance of the dynamic pressures of the two mixing gases.

A study was made to determine the effects of various physical phenomena on the plume gas density and electron density distributions in order to define a proper plume model in which the significant physical phenomena are included. The results are presented below.

#### 3.3.1 Approximate Far-Field Plume Models

A number of semi-empirical plume models are available to compute the plume flow field when atmospheric interaction can be neglected. These approximate models have been successfully applied to the far field of the plume but become inaccurate as the nozzle exit is approached and the near field expansion of the nozzle flow is felt.

Two such models were investigated for the MX third stage vacuum plume application, viz., the Brook model<sup>17</sup> and the Boynton model.<sup>18</sup> The former model, however, requires some adjustment of parameters to match an exact solution so that it is difficult to apply from knowledge of the rocket engine characteristics alone.

In the Brook model, the plume density is computed from

$$\bar{\rho}\bar{V}\bar{r}^2 = F(\bar{r},m)\exp -\lambda^2(1-\cos\theta)^m \quad (3)$$

with

$$\bar{\rho} \equiv \rho/\rho_0, \quad \bar{V} \equiv V/V^*, \quad \bar{r} \equiv r/R_e \quad (4)$$

where

$\rho_0$  = stagnation density

$V^*$  = sonic velocity at the nozzle throat

$R_e$  = nozzle exit radius

$r$  = radial distance from the nozzle

$\theta$  = polar angle

The  $\lambda$  depends on the rocket engine and nozzle characteristics, and  $m$  is a parameter to be matched to an exact solution. Along the plume axis,  $\theta = 0$  and Eq. (1) becomes

$$\bar{\rho} \bar{V} \bar{r}^2 = F(\bar{r}, m) \quad (5)$$

From a method of characteristics solution for uniform flow properties at the nozzle exit plane (i.e., with the particulate effects in the nozzle flow neglected), the function  $F$ , which represents the mass flow per unit solid angle along the plume axis, is evaluated and the parameter  $m$  in Eq. (5) is adjusted to yield the best fit (see Fig. 21). Note that  $m = 0.825$  provides the best fit to the exact solution in the far field, and large errors are expected for small  $\bar{r}$ . With the parameter  $m$  fixed, the plume density can be computed from Eq. (3) and any other flow properties computed from isentropic relations.

The Boynton model gives the following expression for the plume density:

$$\rho = \pi c \rho^* \left( \frac{V^*}{V_m} \right) \left( \frac{r}{R^*} \right)^{-2} \cos^{\frac{2}{\gamma-1}} \left( \frac{\pi}{2} \frac{\theta}{\theta_\infty} \right) \quad (6)$$

with

$$c = \frac{1}{2\pi} \left( \frac{\gamma+1}{\gamma-1} \right) \left( \frac{\pi}{2\theta_\infty} \right)^2 \quad (7)$$

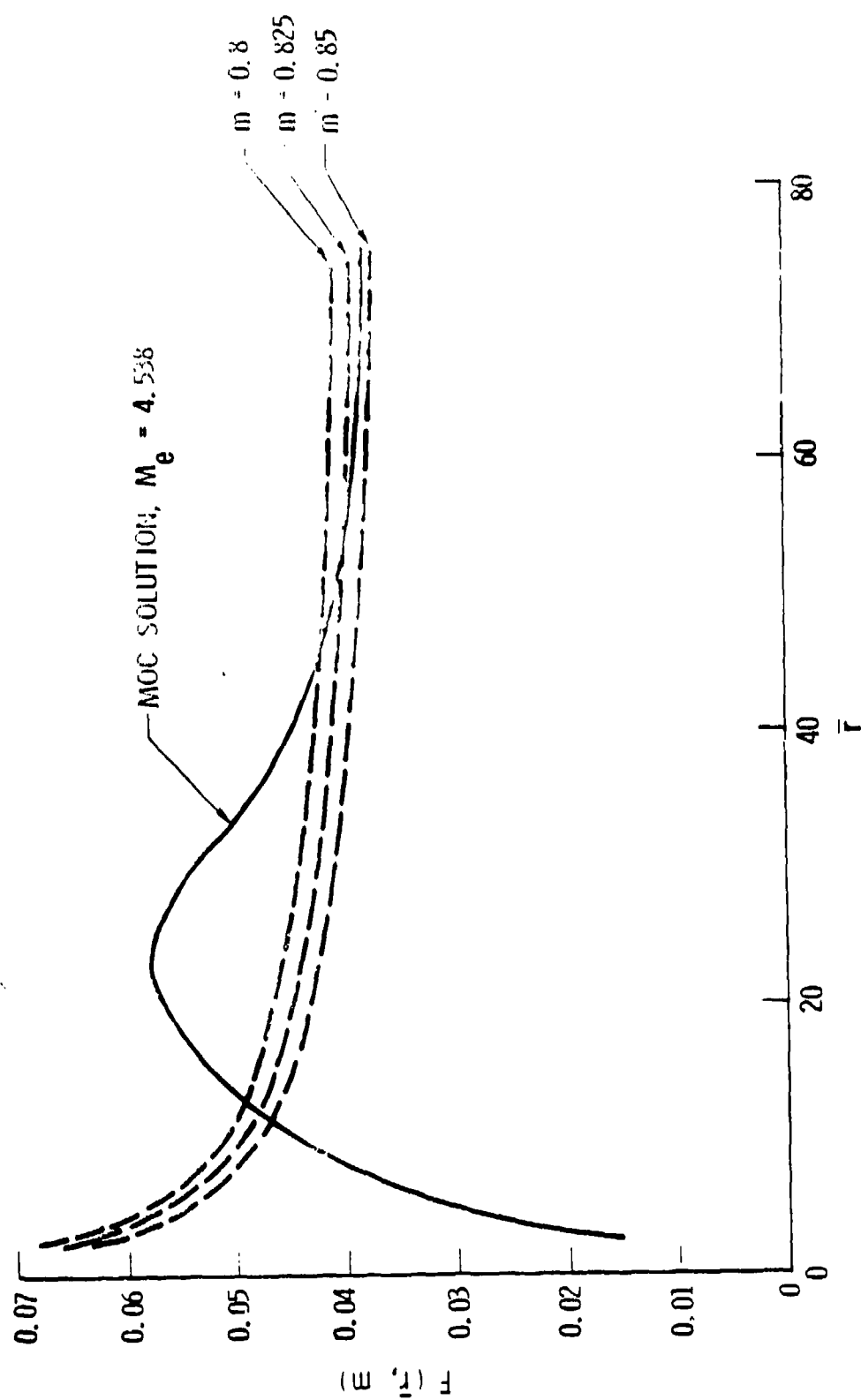


Fig. 21. Mass Flow Along  $\bar{r}$  Third Stage Plume Axis

where

$V_m$  = limiting gas velocity

$\theta_m$  = maximum Prandtl-Meyer turning angle

$\rho^*$  = density at the nozzle throat

$V^*$  = sonic velocity at the nozzle throat

$R^*$  = throat radius

The constant  $C$  is close to 1, and for the present case  $C = 0.816$ .

In Fig. 22, predictions of the constant electron density contours from the two approximate models are compared to the exact solution for the MX third stage plume with uniform nozzle exit properties and exit electron mole fraction of  $8.6 \times 10^{-7}$ . The contours labeled  $n_e = 2.156 \times 10^9$  correspond to the over-dense boundary for the UHF command-destruct frequency of 416.5 MHz. It is evident that the Brook model yields better agreement with the exact solution.

These studies indicate that for liquid rocket engines where the amount of particulate in the exhaust is nil or insignificant, the approximate vacuum plume models will provide quick and simple estimates of the plume electron density distributions. However, when large amounts of particulates are present, as in the case of solid rocket engines, the nozzle exit flow properties are nonuniform. They cannot be accounted for by the approximate models, and numerical solutions must be found.

### 3.3.2 Effect of Particulates on Plume Electron Density

A study was made to evaluate the effect of the presence of solid particles in the MX third stage plume on the gas density and electron density distributions. The nozzle exit plane flow properties as shown in Figs. 18 and 19

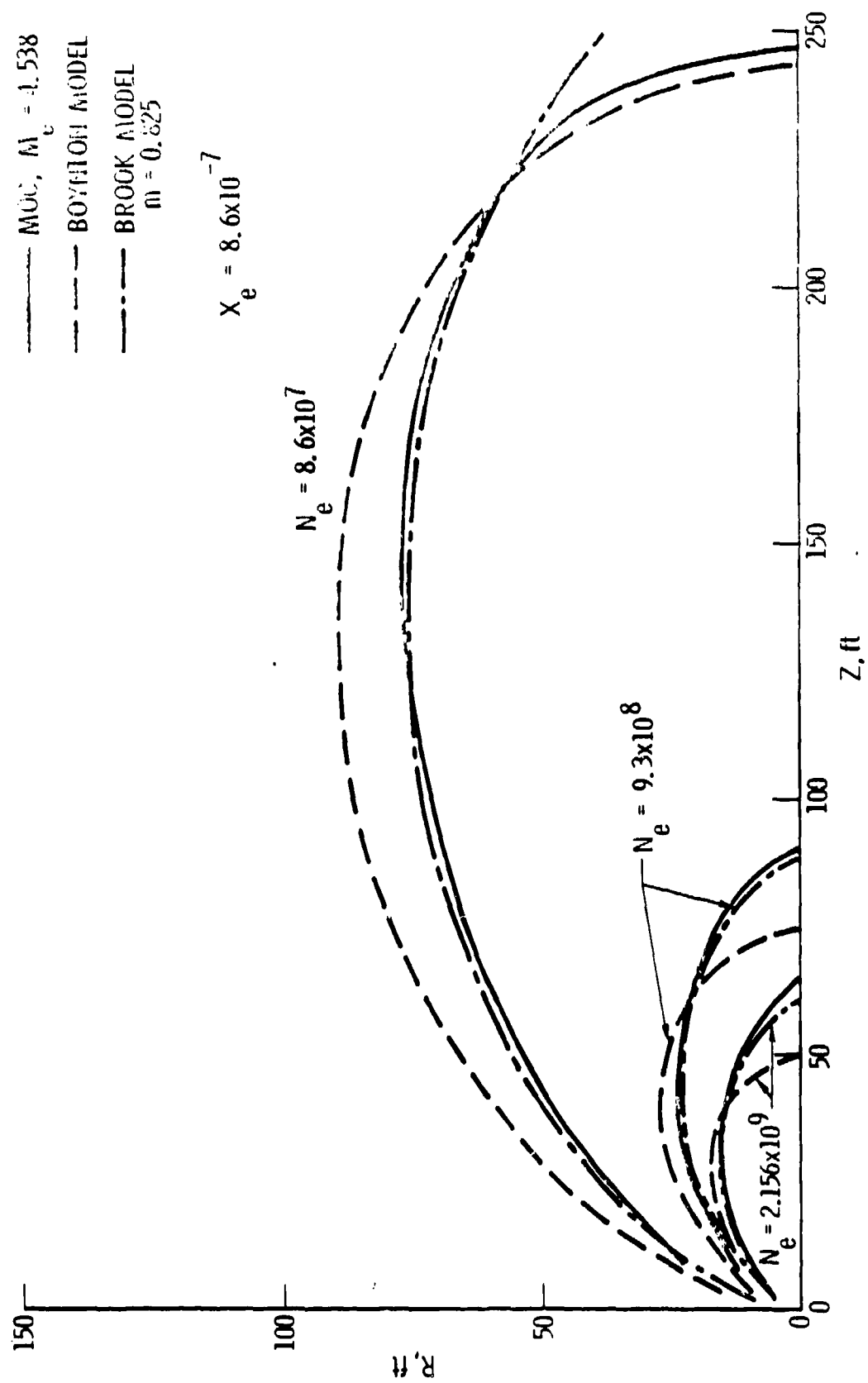


Fig. 22. Contours of Constant Electron Density for Uniform Exit Mach Number



were used to continue the plume flow field calculation utilizing both the TD2P and the MOC code. The latter code solves the inviscid equations of motion for the gas phase only. The results are converted into electron density contours and are presented in Fig. 23.

Apparently, the presence of 30 percent  $Al_2O_3$  particles in the plume has only a small effect on the electron density distribution. The particulates cause large changes in the gas properties of the rocket nozzle, as shown previously, because of exchange of heat and momentum between the two phases. This effect was included in all the results presented in Fig. 23. When the rocket exhaust expands into a much lower pressure outside the nozzle, the gas density is greatly reduced. As a result, the heat and momentum transfer between the two phases quickly ceases, and the gas and particle motions become essentially independent of each other. The close agreement between the gas-only and the two-phase flow solutions demonstrated this decoupling of the motions of the two phases.

As the two-phase plume calculation is more complex and time-consuming than the gas-only calculation, the latter approach appears more attractive and economical and should generate electron density distribution of sufficient accuracy for the subsequent RF interaction calculation. For these reasons, results shown in the remainder of this report were generated for the gas phase plume only.

However, the presence of the particulates affects the plume density and electron density distributions through their interaction with the gas phase in the rocket nozzle to produce nonuniform nozzle exit properties as shown previously. This is shown in Fig. 24 where gas plume calculations were made at the 310 kft altitude, using both the constant and the nonuniform flow properties in Figs. 18 and 19 as inputs. The latter properties reflect the effects of the particulates. At the 310 kft altitude, the atmosphere is sufficiently dense to confine the plume to within the plume boundary as shown in Fig. 24 with the generation of the barrel shock interior to the boundary. Figure 24 shows that the presence of the particulates in the nozzle increases the plume size and

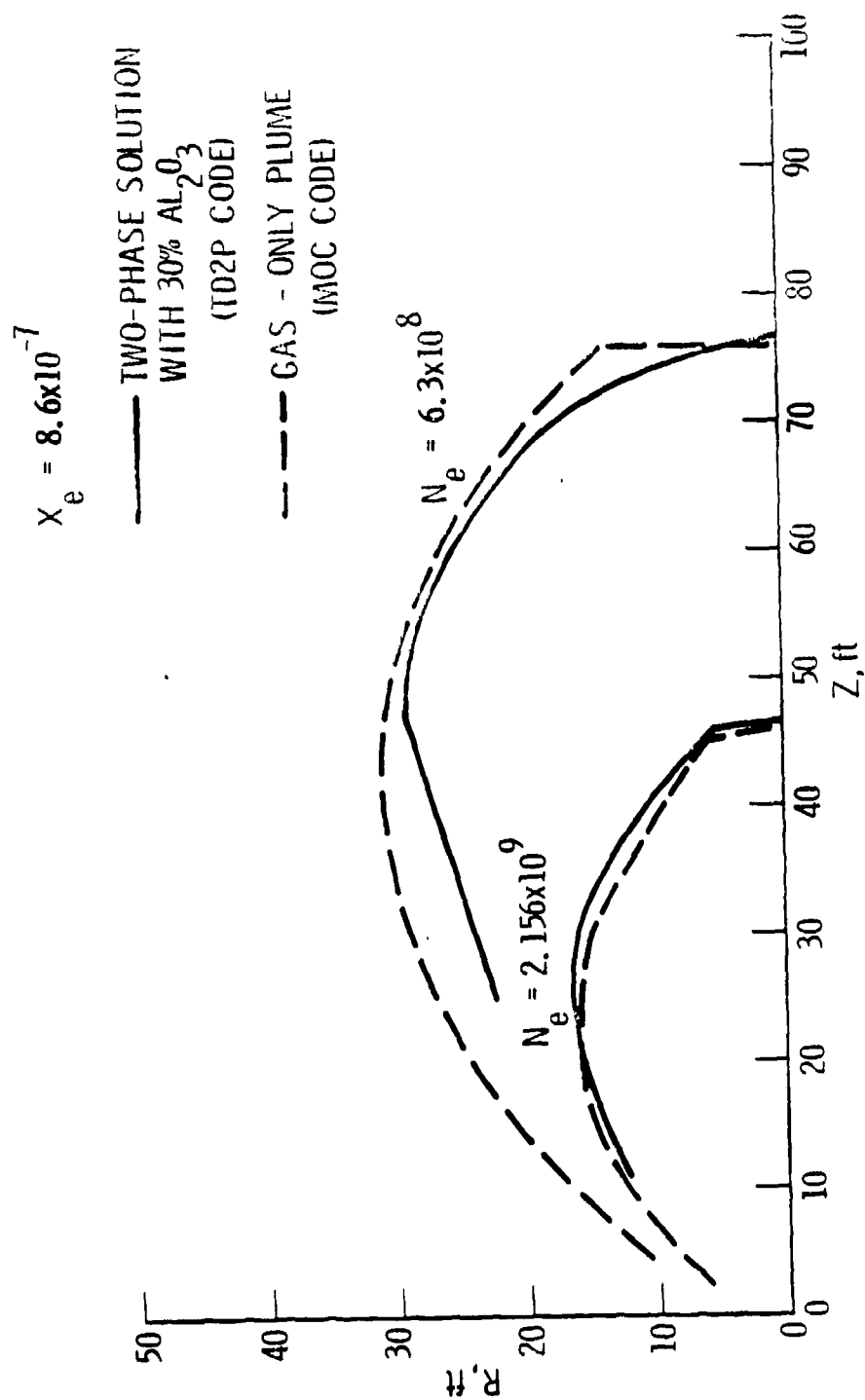


Fig. 23. Electron Density Contours for Gas and Two-Phase Plume

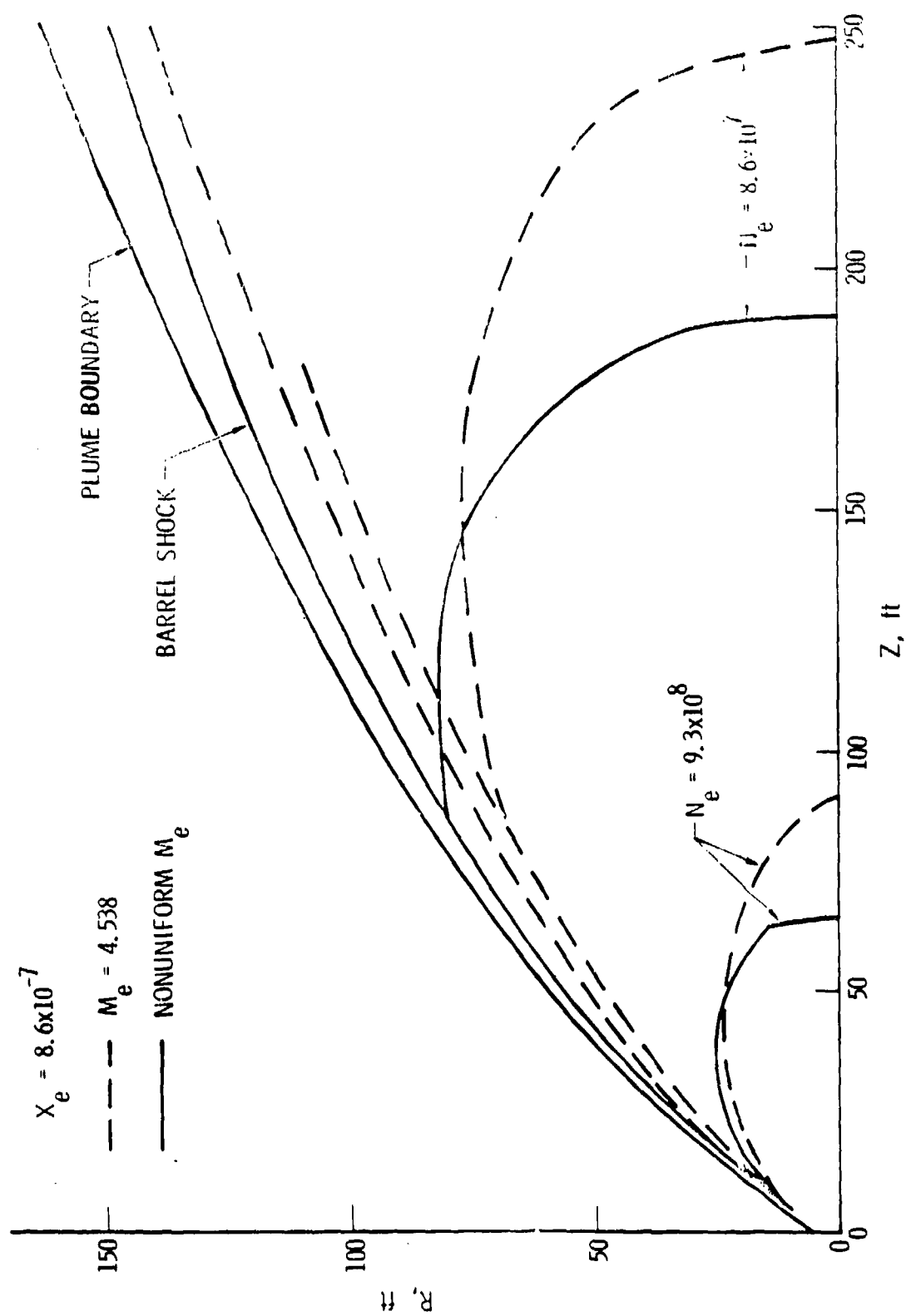


Fig. 24. Effect of Two-Phase Nozzle Flow on Gas Plume at 310 kft

causes significant changes in the gas density and electron density distributions. For solid rocket engines, therefore, a two-phase flow calculation in the rocket nozzle should be made to account for the effects of the particulates.

### 3.3.3 Effect of External Atmosphere

When the ignition altitude of the rocket engine is sufficiently low, such as for the BOA-3 trajectory of the planned MX test flight where the third stage ignites at 259 kft, interaction with the surrounding atmosphere causes the plume to be confined. The plume boundary will increase with altitude until the atmospheric density is so small that the plume can be considered to be expanding into a vacuum. Figure 25 demonstrates this atmospheric effect. The shaded portion depicts the overdense region at the UHF command-destruct frequency where RF signals are totally reflected. In addition to the overdense core, there exists an overdense region between the plume boundary and the barrel shock due to the gas density increase across the barrel shock. The maximum diameter of the shock-layer overdense region increases with altitude and then decreases until at some altitude the shock layer is no longer overdense and only the overdense core remains. For the MX third stage this is estimated to be at about 310 kft. Below this altitude, the atmospheric effect should be considered. However, this effect occurs only within a small portion of the entire ignition altitude region. Its impact on the overall range safety operation needs more careful evaluation.

### 3.3.4 Effect of Nozzle Wall Boundary Layer

As the rocket exhaust flows through the nozzle, a thin boundary layer near the nozzle wall is generated. For the large thrust levels generally employed for the various stages of the launch vehicle, the boundary layer is usually turbulent. The Mach number in the boundary layer decreases from supersonic at the boundary layer edge to subsonic near the nozzle wall. Because of the lower Mach number and its proximity to the wall, the gas in the boundary layer expands to much larger angles than the rest of the exhaust gas once it

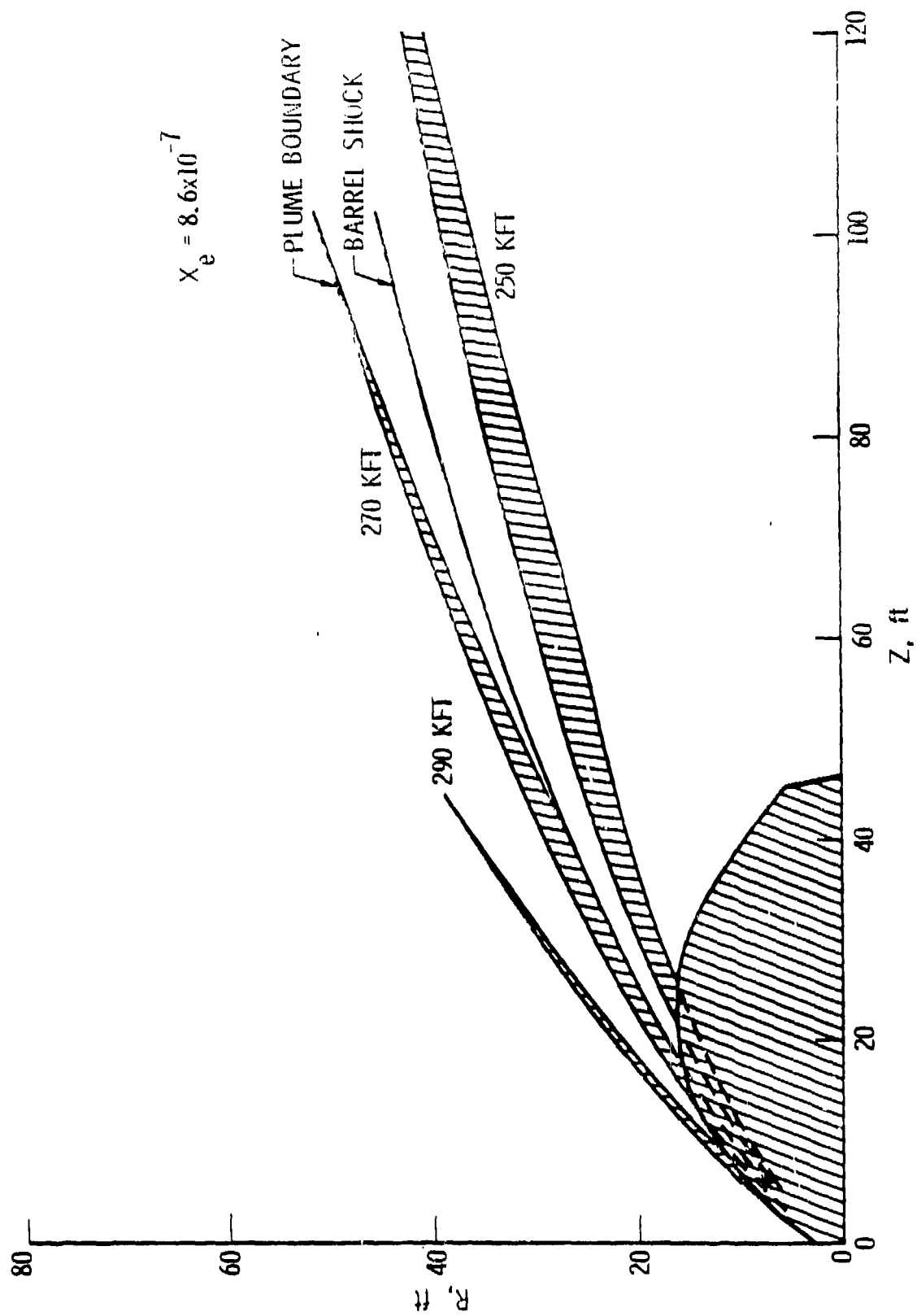


Fig. 25. Atmospheric Effect of UHF Overage Contour

exits from the nozzle. The presence of the boundary layer, however, is not expected to alter the electron density significantly in those regions of the plume where RF interaction is appreciable, since the electron density in that part of the plume which originates from the boundary layer is much lower than in the interior of the plume because of the large angle expansion of the boundary layer gas. Nevertheless, the effect of the boundary layer was investigated by computing the inviscid expansion of the boundary layer with the MOC code.

In Fig. 26, results with and without the presence of the nozzle boundary layer are compared. It is evident that the boundary layer effect is insignificant. Although not shown in the figure, the electron density distributions for the two cases are nearly identical. It is concluded that for RF-plume interaction analysis the presence of the nozzle boundary layer can be neglected.

### 3.3.5 Effect of Nozzle Length

In the study of the MX third stage plume effects on RF signal propagation, the effect of nozzle extension was considered. In the stowed configuration before the second and third stage separation, the third stage nozzle measures 36.5 in. from the throat. The nozzle is extended to 75.0 in. when the third stage is deployed. The plume flow field was computed for both nozzle lengths to determine the difference in the electron density distribution. The results are presented in Fig. 27. The exhaust plume from the unextended nozzle has a smaller UHF overdense core. This is mainly due to the lower electron mole fraction in the exhaust gas from the unextended nozzle as shown by the electron mole fraction variation along the nozzle in Fig. 4. Some displacements of the plume boundary and the barrel shock are also noted. However, the change in the plume shape is small.

These results imply that the exhaust plume from the fully extended nozzle will cause greater RF interaction and should be chosen as the more conservative case.

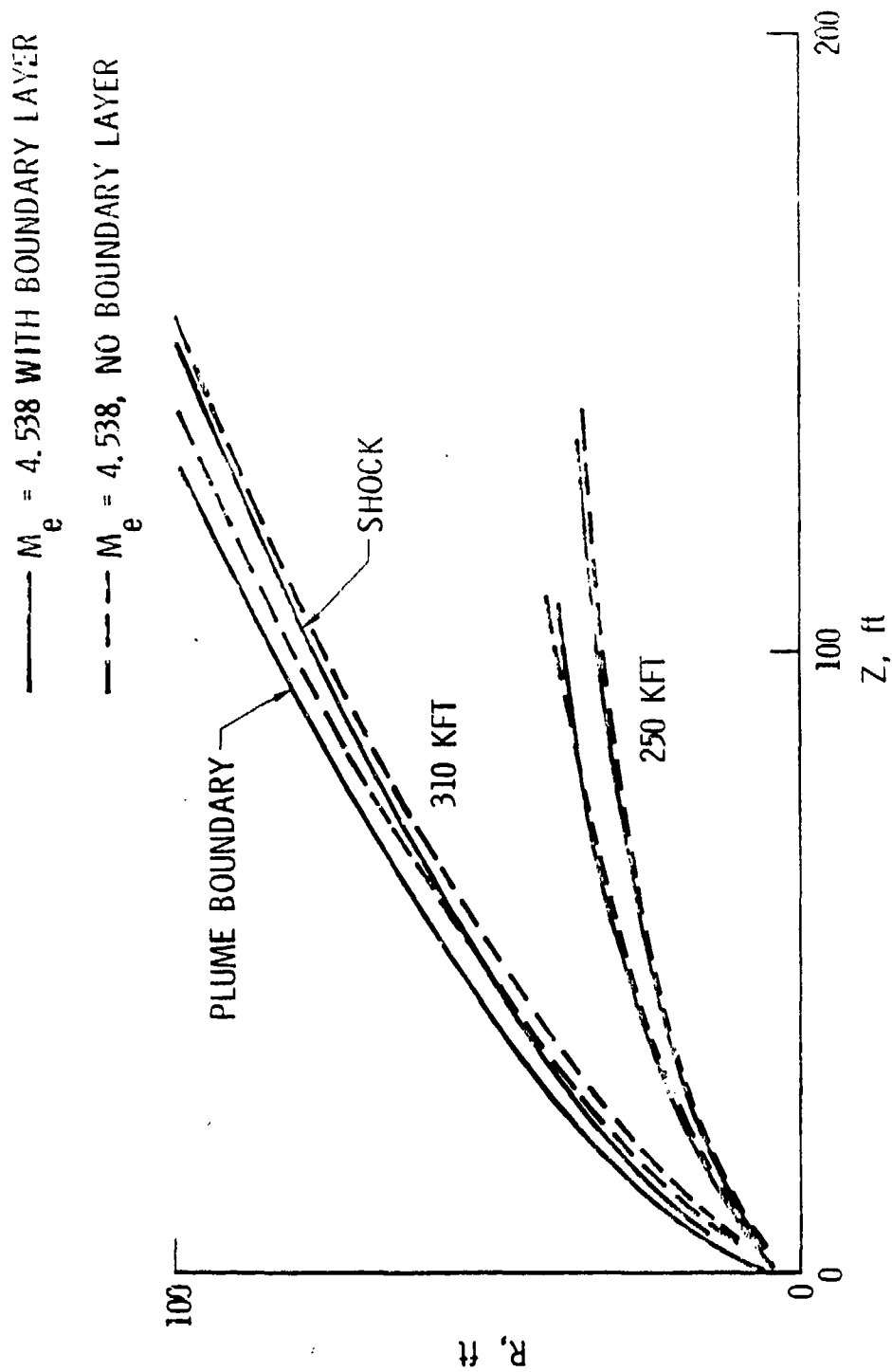


Fig. 26. Effect of Nozzle Boundary Layer

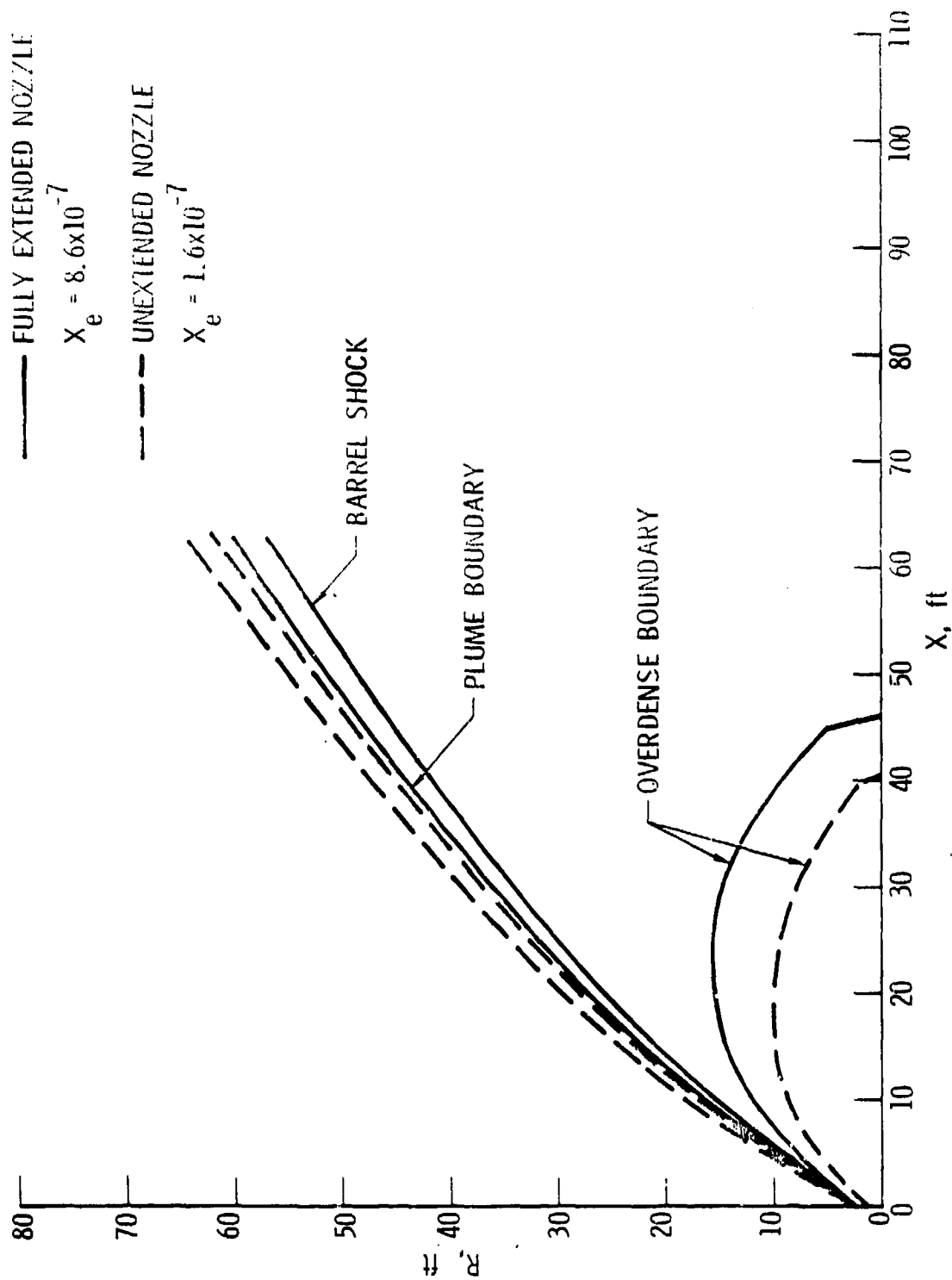


Fig. 27. UHF Overdense Contour of MX Third Stage Plume at 310 kft



#### 4. CONCLUSIONS

For the purpose of determining the effects of a rocket exhaust plume on RF signal propagation, it is necessary to provide plume flow field properties, such as gas density, electron density, and temperature distributions, from theoretical prediction. From studies of the various factors which influence the ionization and gas density distributions in the exhaust plume of a solid rocket engine, the following conclusions are obtained:

- o Electrons in the rocket exhaust are generated by ionization of the alkali contaminants in the rocket chamber. The ionization level changes as the exhaust flows through the nozzle due to additional reactions among the ionic species, with the two-body attachment reaction  $\text{HCl} + e = \text{H} + \text{Cl}^-$  being predominant in controlling the ionization level. Based upon the present knowledge of its reaction rate, a factor of seven uncertainty in the plume electron density distribution can be expected.
- o The particulate matters in the two-phase exhaust affect the plume electron density distribution mainly through their effects on the nozzle flow field as they interact with the gas phase in the exchange of heat and momentum. Their presence in the plume flow field can be neglected in the determination of electron density distribution due to the weak interaction between the particulates and the plume gas.
- o In the altitude range below 310 kft, the plume shock formed by the interaction of the MX third stage exhaust with the surroundings causes the appearance of an outer UHF overdense region which should be considered in the calculation of RF signal degradation.
- o The presence of the nozzle wall boundary layer has a negligible effect on the plume plasma properties and the RF signal propagation.

- o The exhaust from the fully extended nozzle of the MX third stage presents a more severe plasma environment to RF signal propagation than that of the unextended nozzle.
  
- o Approximate far field plume models, such as the Brook model and the Boynton model, may be useful for the description of plumes from liquid rocket engines. They cannot account for the interaction between the particulates and the gas in the rocket nozzle and are not accurate enough to describe plumes from solid rocket engines.

## REFERENCES

1. Victor, A.C., "Plume Signal Interference, Part 1: Radar Attenuation," Report NWC-TP-5319, Part 1, Naval Weapons Center, China Lake, CA, June 1965.
2. Victor, A.C., "Plume Signal Interference, Part 1: Plume-Induced Noise (U)," Report NWC-TP-5319, Part 2, Naval Weapons Center, China Lake, CA, June 1975 (Confidential).
3. Poehler, H.A., "Results of Special Flame Measurements of Titan III-C Tests 3656/6025 and 6020/6546," Report ETV-TRM-66-30, Pan American World Airways, Guided Missile Range Division, 1966.
4. Poehler, H.A., "Project See-Thru, Flame Attenuation Interference Measurements, Titan III-C Test 8275/2250, Preliminary Report," Report No. ETR-TR-68-6, Pan American World Airways, 1967.
5. Poehler, H.A., "Project See-Thru, Flame Interference Measurements, Titan III-C Launch Test 8275/2250, Final Report," Report No. ETR-TR-68-3, Pan American World Airways, 1968.
6. Poehler, H.A., "Rocket Exhaust Signal Attenuation and Degradation, Final Report, Vols. I, II, III," Report No. ETR-TR-69-4, Pan American World Airways, Aerospace Service Division, 1969.
7. Ely, O.P., "Rocket Exhaust Effects on Radio Frequency Transmission," J. Spacecraft, 3, pp. 310-314, 1966.
8. Vicente, F.A., E.C. Taylor, and R.W. Phelps, "Analysis of Flame Effects on Measuring Electromagnetic Propagation Data," J. Spacecraft, 4, pp. 1069-1075, 1967.
9. Golden K.E., E.L. Taylor, and F.A. Vicente, "Diffraction by Rocket Exhaust," Communication in IEEE Transaction in Antenna and Propagation, AP16, pp. 614-616, 1968.
10. "Post Launch Analysis Telemetry Systems Preview--Operation 3162," Report No. PA300-T-79-31P, Systems Performance Analysis Department, Western Test Range Division, Federal Electric Corporation, 26 July 1979.
11. "Post Launch Analysis of Telemetry Systems--Operation 5544, Final," Report No. AS300-T-81-21F, Systems Performance Analysis Department, Western Test Range Division, Federal Electric Corporation, 1 April 1981.
12. McKelvey, G.R., "Exhaust Plume Test Results--Report Number 2," Technical Note PA300-N-79-23, Systems Performance Analysis Department, Western Test Range Division, Federal Electric Corporation, 27 September 1979.

# REFERENCES (Continued)

13. Sutton, G.A., "Boost Measurements and Analysis Program Final Report, Vol. 7: Plasma Properties Derived From Full Scale Rocket Motor Measurements," Ford Aerospace and Communications Corporation Report No. J-6111, prepared by Concord Sciences Corporation, Concord, MS, 15 March 1979.
14. August G. and D. Tremain, "Boost Measurements and Analysis Program Final Report, Vol. 9: Rocket Plume Measurements and Data Evaluation," Ford Aerospace and Communications Corporation Report No. U-6511, prepared by Concord Sciences Corporation, Concord, MS, 15 March 1979.
15. Chang, I-S., "Three-Dimensional, Two-Phase Supersonic Nozzle Flows," AIAA Paper No. 81-1219, AIAA 14th Fluid and Plasma Dynamics Conference, Palo Alto, CA, 23 June 1981.
16. Hill, A.F.J. and J.S. Draper, "Analytical Approximation for the Flow from a Nozzle into a Vacuum," J. Spacecraft, 3, pp. 1552-1554, 1966.
17. Brook J.W., "Far Field Approximation for a Nozzle Exhausting into a Vacuum," J. Spacecraft, 6, pp. 626-628, 1969.
18. Boynton, F.P., "Exhaust Plumes from Nozzles with Wall Boundary Layers," J. Spacecraft, 5, pp. 1143-1147, 1968.
19. Smith S.D. and A.W. Tatliff, "Rocket Exhaust Plume Computer Program Improvement, Volume IV: Final Report," Report No. LMSC/HREC D162220-IV-A, Lockheed Missiles and Space Company, Huntsville, AL, June 1971.
20. Penny, M.M., et al., "Supersonic Flow of Chemically Reacting Gas-Particle Mixtures, Volume I: A Theoretical Analysis and Development of the Numerical Solution," Report No. LMSC/HREC TR D496555-I, Lockheed Missiles and Space Company, Huntsville, AL, January 1976.
21. Penny, M.M., et al., "Supersonic Flow of Chemically Reacting Gas-Particle Mixtures, Volume II: RAMP--A Computer Code for Analysis of Chemically Reacting Gas-Particle Flows," Report No. LMSC/HREC TR D496555-II, Lockheed Missiles and Space Company, Huntsville, AL, January 1976.
22. Kliegel, J.R. and G.R. Nickerson, "Axisymmetric Two-Phase Perfect Gas Performance Program, Volume I: Engineering and Program Description," Report No. 02784-6006-R000, TRW, 3 April 1967.
23. "User's Manual for the Two-Dimensional Two-Phase Plume Analysis Computer Program," Report No. SN-141, Dynamic Sciences, Inc., December 1968.

#### REFERENCES (Concluded)

24. Romine, G.L., et al., "RF Signal Degradation from the MX Stage III Plume," Report No. SE4-116037, Martin-Marietta Corporation, Denver, CO, May 1981.
25. Heald, M.A. and C.B. Wharton, Plasma Diagnostics with Microwaves, John Wiley & Sons, Inc., New York, NY, p. 6, 1965.
26. Malmud, P., "Raybend--A Tracing Program for Microwaves Propagating through Rocket Plumes," paper presented at the JANNAF 12th Plume Technology Meeting, October 1980.
27. Born & Wolf, Principles of Optics, Pergamon Press, London, p. 110, 1959.
28. Vicente, F.A., E.C. Taylor, and R.W. Phelps, "Analysis of Flame Effects in Measured Electromagnetic Propagation Data," J. Spacecraft, 4, pp. 1069-1075, 1967.
29. Peng, S.Y., "Analytical Model for Predicting R-F Amplitude and Phase Effects of Plume," JANNAF 10th Plume Technology Meeting, 1977.
30. Boynton, F.W., A.R. Davies, P.S. Rajasckhar, and J.A. Thompson, "Effects of Large Absorbing Rocket Exhaust Plumes on R.F. Signals," JANNAF 10th Plume Technology Meeting, CPI Publications 291, pp. 143-173, 1977.
31. Jensen, D.E. and G.A. Jones, "Gas-Phase Reaction Rate Coefficients for Rocketry Applications," Rocket Propulsion Establishment Report No. 71/9, Ministry of Defense, London W.C. 2, October 1971.
32. Radke, H.H., L.J. Delaney, and P. Smith, "Exhaust Particle Size Data from Small and Large Solid Rocket Motors," Report No. TOR-1001 (S2951-18)-3, The Aerospace Corporation, El Segundo, CA, July 1967.

APPENDIX  
CHEMICAL REACTIONS IN ROCKETRY APPLICATION  
(gmole-cm-sec units)

No.	Reactions	$A$	$n$	$E$ (kcal/ mole)	Uncertainty Factor	
					Upper Bound*	Lower Bound**
1.	$M + H + OH = H_2O + M$	$7.5 \times 10^{23}$	2.6	0.	10	10
2.	$M + H + H = H_2 + M$	$6.4 \times 10^{17}$	1.0	0.	30	30
3.	$M + CO + O = CO_2 + M$	$1.38 \times 10^{34}$	5.24	5.6	3	30
4.	$M + H + Cl = HCl + M$	$3.0 \times 10^{16}$	0.5	0.	100	100
5.	$M + AlCl + Cl = AlCl_2 + M$	$3.0 \times 10^{16}$	0.5	0.	100	100
6.	$M + AlCl_2 + Cl = AlCl_3 + M$	$3.0 \times 10^{16}$	0.5	0.	100	100
7.	$H_2 + OH = H + H_2O$	$2.19 \times 10^{13}$	0.	5.15	3	3
8.	$CO + OH = CO_2 + H$	$5.6 \times 10^{11}$	0.	1.08	5	5
9.	$HCl + OH = H_2O + Cl$	$10^{11}$	-0.5	6.0	30	30
10.	$AlCl_2 + H = AlCl + HCl$	$1.05 \times 10^{11}$	-0.5	2.566		
11.	$Cl_2 + H = HCl + Cl$	$3.0 \times 10^{14}$	0.	3.0	5	5
12.	$CO + O = CO_2$	$1.78 \times 10^{10}$	0.	2.53		
13.	$Al + HCl = AlCl + H$	$5.0 \times 10^{11}$	-0.5	5.673		
14.	$AlO + HCl = AlOCl + H$	$10^{11}$	-0.5	5.673		
15.	$AlCl + OH = AlOCl + H$	$10^{11}$	-0.5	5.619		
16.	$AlOH + OH = H + AlO_2$	$10^{11}$	-0.5	5.627		
17.	$K + HCl = KCl + H$	$3.612 \times 10^{14}$	0.	5.0	10	30
18.	$Na + HCl = NaCl + H$	$3.01 \times 10^{14}$	0.	8.0	10	30
19.	$M + K^+ + e = K + M$	$7.25 \times 10^{25}$	1.5	0.	5	5

\* Factor by which the rate is increased

\*\* Factor by which the rate is decreased

<u>No.</u>	<u>Reactions</u>	<u>A</u>	<u>n</u>	<u>E</u> (kcal/ mole)	<u>Uncertainty Factor</u>	
					<u>Upper Bound*</u>	<u>Lower Bound**</u>
20.	$M + Na^+ + e = Na + M$	$5.435 \times 10^{17}$	2.0	0.	5	5
21.	$M + Cl + e = Cl^- + M$	$1.09 \times 10^{18}$	0.	0.	30	30
22.	$K^+ + Cl^- = K + Cl$	$6.02 \times 10^{15}$	0.5	0.	10	100
23.	$Na^+ + Cl^- = Na + Cl$	$1.81 \times 10^{16}$	0.5	0.	10	100
24.	$HCl + e = H + Cl^-$	$6.02 \times 10^{15}$	0.	19.37	30	100

The symbol M in the three-body reactions denotes any chemical species present in the system. The species have different catalytic efficiencies of causing the reaction to proceed during collisions. The factors listed below for Reactions 1 and 2 are used to multiply the individual concentration before their concentrations are summed in the reaction rate calculation. For all other reactions, a catalytic efficiency of 1 is used.

#### Catalytic Efficiencies for Three-Body Reactions

<u>Reactions</u>	<u>Species</u>						
	<u>H<sub>2</sub>O</u>	<u>H<sub>2</sub></u>	<u>H</u>	<u>O</u>	<u>OH</u>	<u>CO</u>	<u>CO<sub>2</sub></u>
1	20	5	12.5	12.5	12.5	8	8
2	20	4	25.0	25.0	25.0	4	4